HHS Public Access

Author manuscript

Mol Cell. Author manuscript; available in PMC 2024 January 05.

Mechanism of Lys6 poly-ubiquitin specificity by the *L. pneumophila* deubiquitinase LotA

Gus D. Warren[1], **Tomoe Kitao**[2,*], **Tyler G. Franklin**[1,*], **Justine V. Nguyen**[1], **Paul P. Geurink**[3], **Tomoko Kubori**[2,4], **Hiroki Nagai**[2,4], **Jonathan N. Pruneda**[1,‡]

[1]Department of Molecular Microbiology & Immunology, Oregon Health & Science University, Portland, OR 97239, USA

[2]Department of Microbiology, Graduate School of Medicine, Gifu University, Gifu, Gifu 501-1194, Japan

[3]Oncode Institute & Department of Cell and Chemical Biology, Leiden University Medical Centre, Leiden, The Netherlands

[4]G-CHAIN, Gifu University, Gifu, Gifu 501-1194, Japan

SUMMARY

The versatility of ubiquitination to control vast domains of eukaryotic biology is due, in part, to diversification through differently-linked poly-ubiquitin chains. Deciphering signaling roles for some chain types, including those linked via K6, has been stymied by a lack of specificity among the implicated regulatory proteins. Forged through strong evolutionary pressures, pathogenic bacteria have evolved intricate mechanisms to regulate host ubiquitin during infection. Herein, we identify and characterize a deubiquitinase domain of the secreted effector LotA from *Legionella pneumophila* that specifically regulates K6-linked poly-ubiquitin. We demonstrate the utility of LotA for studying K6 poly-ubiquitin signals. We identify the structural basis of LotA activation and poly-ubiquitin specificity, and describe an essential "adaptive" ubiquitin-binding domain. Without LotA activity during infection, the *Legionella*-containing vacuole becomes decorated with K6 poly-ubiquitin as well as the AAA ATPase VCP/p97/Cdc48. We propose that LotA's deubiquitinase activity guards *Legionella*-containing vacuole components from ubiquitin-dependent extraction.

Graphical Abstract

‡Lead contact. Address correspondence to Jonathan N. Pruneda (pruneda@ohsu.edu).
*These authors contributed equally

AUTHOR CONTRIBUTIONS

Conceptualization, JNP; Investigation, GDW, TKi, TGF, JVN, TKu, and JNP; Resources, PPG; Writing – original draft, GDW and JNP; Writing – review & editing, GDW and JNP; Supervision, TKu, HN, and JNP; Funding acquisition, TKu and JNP.

CONFLICT OF INTEREST STATEMENT

JNP, TGF, and JVN are inventors on a licensed technology using LotA to study K6 polyubiquitin. The other authors declare no competing interests.

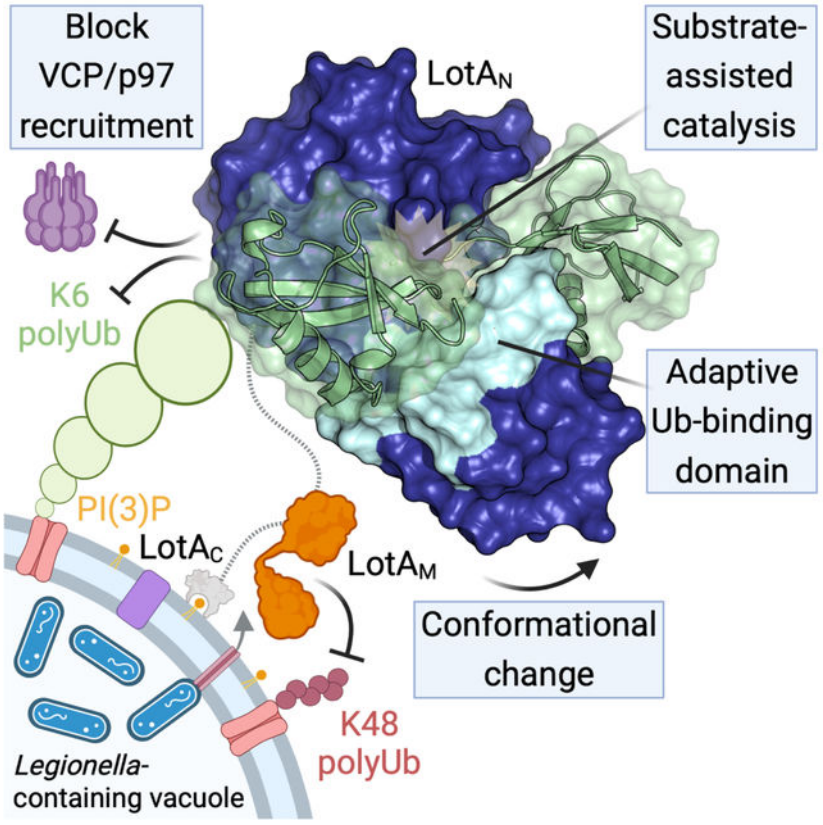

eTOC:

Warren et al. identify a K6-specific deubiquitinase within the *Legionella pneumophila* effector LotA and demonstrate its utility as a research tool. Structural and biochemical work explain the mechanism of LotA activation and specificity. During infection, LotA's deubiquitinase activity guards the *Legionella*-containing vacuole from K6 poly-ubiquitin and VCP recruitment.

Keywords

Ubiquitin; Deubiquitinase; Legionella pneumophila; Bacterial effector; VCP/p97/Cdc48

INTRODUCTION

Post-translational regulation with the small protein modifier ubiquitin (Ub) is essential to all eukaryotic life[1]. In humans, hundreds of enzymes tightly regulate protein ubiquitination by defining both the target substrate and the type of modification[2]. Unlike binary "on-off" modifications such as phosphorylation or acetylation, the Ub signal can be further diversified through the formation of polymeric Ub (polyUb) chains in which any of the seven Lys residues (e.g., K48- or K63-linked chains) or the amino-terminus (linear/M1-linked chains) are ubiquitinated. Differently-linked polyUb chains code for distinct signaling outcomes, including proteasomal degradation (K48-linked chains), the DNA damage response (K63-linked chains), or innate immune signaling (M1-linked chains)[3]. Although

the existence and importance of all eight possible chain types has been established[4–7], signaling outcomes and regulators for half (K6, K27, K29, and K33) remain ill-defined and have thus been coined “atypical” chains[8].

Among atypical chain types, K6-linked polyUb has remained particularly enigmatic. Whether K6 polyUb serves as a proteasomal degradation signal remains unclear, as levels of K6 chains show little or no increase upon proteasomal inhibition[5,9]. K6 polyUb accumulates following mitochondrial depolarization, UV-induced DNA damage, or inhibition of the AAA ATPase VCP/p97/Cdc48[10–13]. Defining the importance of K6 polyUb in these responses, however, has been clouded by the imprecise specificities of the implicated E3 ligases and deubiquitinases (DUBs). Mitophagy, for example, can be regulated by the E3 ligase Parkin and DUBs USP30 and USP8, and while these enzymes can control levels of K6 polyUb, they also target other chain types including K11, K48, and K63[10,14–17]. The same is true for the ligase activity of BRCA1 in the DNA damage response[18–20], as well as the ligase activity of HUWE1 in targeting substrates for VCP[12,13,21]. Confidently ascribing a signaling function for K6 polyUb, therefore, awaits discovery of new approaches or enzymes that can more specifically measure and/or perturb it. Such was the case with M1-linked polyUb, prior to the discovery of M1-specific regulators[22].

PolyUb chain specificity is typically achieved through the concerted action of multiple Ub-binding sites. E2 Ub-conjugating enzymes and E3 ligases achieve linkage specificity through specific coordination of two Ub molecules[23]. Within the resulting polyUb chain, Ub molecules are classified as a distal Ub (Ub^{dist}) that is linked via its C-terminus onto an amino group of the proximal Ub (Ub^{prox}). For DUBs, specificity is often achieved via Ub-binding sites that oppose the catalytic center, including an S1 site that binds Ub^{dist} and an S1’ site that binds Ub^{prox} in a linkage-specific orientation[24]. Linkage-specific regulators have been identified for M1, K11, K48, and K63 polyUb[3], but despite considerable efforts, human enzymes with stringent specificity toward K6 polyUb have thus far evaded detection.

Pathogenic bacteria represent an alternative source of polyUb linkage-specific enzymes. Bacterial pathogens have evolved Ub regulatory enzymes that interfere with human signaling processes during infection, including a number that target specific polyUb chain types[25]. In fact, NleL from enterohemorrhagic *Escherichia coli* is the most K6-specific ligase known to-date, assembling a 50:50 mixture of K6 and K48 linkages[26]. The causative agent of Legionnaires’ disease, *Legionella pneumophila*, has evolved numerous mechanisms of disrupting or hijacking host Ub signaling. Of the >300 effector proteins secreted into infected cells via the *L. pneumophila* Dot/Icm type IV secretion system, several dozen regulate host Ub signals[27], including some that target specific polyUb chain types[28]. Many Ub-targeted *Legionella* effectors localize to the *Legionella*-containing vacuole (LCV), where they edit the complex “coat” of Ub modifications in order to establish a replicative niche and evade host immune responses[29]. One such effector, termed *Legionella* OTU-like protein A (LotA), was reported to contain two catalytic DUB domains with similarity to the human ovarian tumor (OTU) family, as well as DUB activity toward K6, K48, and K63 polyUb[30]. Whether and how one of LotA’s catalytic OTU domains might be specific toward K6 polyUb, however, remained unknown.

Here we demonstrate that the two catalytic DUB modules of LotA are separable and have distinct activities and specificities. Remarkably, the first OTU domain of LotA encodes perfect specificity toward K6 polyUb and represents a valuable tool for studying this atypical linkage. To understand the molecular basis for K6 specificity, we determined crystal structures for LotA alone and bound to K6 diUb. Detailed biochemical analyses revealed a multi-step mechanism of LotA activation that endows K6 specificity, which incorporates themes of conformational rearrangement and substrate-assisted catalysis observed in human linkage-specific DUBs. In the process of studying LotA, we discovered a class of Ub-binding domain that is adapted across the *Legionella* Lot class as well as an otherwise unrelated DUB from *Orientia tsutsugamushi*. During *L. pneumophila* infection, we find that LotA plays a role in clearing K6 polyUb from the LCV, which prevents downstream recruitment of VCP. We propose that the dual DUB activities of LotA act to guard select components of the LCV from Ub- and VCP-dependent extraction. This work provides a powerful tool for the study of Ub biology and firmly establishes an interesting link for K6 polyUb at the host-pathogen interface.

RESULTS

LotA encodes two catalytic DUB domains with distinct specificities

The Lot class of DUBs encoded by *L. pneumophila* is currently composed of LotA (lpg2248), LotB (lpg1621), LotC (lpg2529), and LotD (lpg0227) and defined by a ~100 amino acid insertion within the OTU domain. The Lot-class insertion domains are more diverse in primary sequence than the core OTU domains (Fig. S1A–B), suggesting that they may play a role in determining the various polyUb specificities that have been reported[30–35]. LotA encodes two Lot-class OTU domains, denoted $LotA_N$ and $LotA_M$ for the N-terminal and middle domains, respectively, followed by the C-terminal $LotA_C$ domain that binds PI(3)P, localizing LotA to the LCV during infection[30] (Fig. 1A). As reported previously for shorter polyUb chains[30], we observe that full length LotA is capable of hydrolyzing long polyUb chains composed of a range of different linkage types, including notable activity toward K6-, K48-, and K63-linked substrates (Fig. 1B). The sequence relationship between $LotA_N$ and $LotA_M$ is the most distinct observed among the Lot class, with sequence identities of only 19% and 23% within the insertion and OTU domains, respectively (Fig. S1A–B). To determine if $LotA_N$ and $LotA_M$ contribute distinct activities to that observed for full length LotA (Fig. 1B)[30], we cloned and expressed the isolated domains for biochemical analyses.

Both the $LotA_N$ and $LotA_M$ isolated constructs reacted with the Ub-Propargylamide (Ub-PA) activity-based probe, indicating that each are competent for DUB activity (Fig. 1C)[36]. Reactivities of $LotA_N$ and $LotA_M$ with Ub-PA were ablated by mutation of their annotated catalytic cysteine residues, C13 and C303, to alanine (Fig. 1A,C)[30]. Surprisingly, although both constructs reacted with the monomeric Ub-PA substrate, neither could cleave the monomeric Ub-KG(TAMRA) fluorescent substrate, or the analogous NEDD8, SUMO1, or ISG15 substrates (a discrepancy that will be discussed further below) (Fig. 1D, S1C–E)[37]. When incubated with each of the eight canonical (iso)peptide-linked diUb substrates, $LotA_N$ demonstrated remarkable specificity for the K6 linkage type (Fig. 1E). In contrast, $LotA_M$

was very inefficient and only showed marginal cleavage of the K6-linked substrate at high concentration after a long incubation period (Fig. 1F). As the polyUb chain length has been reported to affect the activities and/or specificities of some DUBs[38–40], we assembled a panel of seven differently-linked tetraUb substrates (lacking only K27). $LotA_N$ again showed exquisite specificity against the K6 linkage, while $LotA_M$ now demonstrated more robust DUB activity, with a distinct preference toward the K48 linkage and lesser activities toward K6 and K63 tetraUb (Fig. 1G–H). Consistent with observations made with the diUb panel (Fig. 1F), $LotA_M$ activity appeared to stall after the tetraUb and triUb were consumed, leaving a diUb product that was stable over time (Fig. 1H). These results indicate that $LotA_N$ and $LotA_M$ indeed demonstrate distinct DUB properties, with $LotA_N$ showing exquisite K6 specificity while $LotA_M$ shows a preference toward longer K48-linked polyUb that is likely directed by an additional (S2 or S2') Ub-binding site. Within the context of full length LotA, the specificity and activity of the $LotA_N$ OTU domain are independent of the $LotA_M$ OTU domain, as a full length LotA C303A variant demonstrates the same K6 specificity and rate of cleavage as the isolated $LotA_N$ construct (Fig. 1I–J).

Benchmarking $LotA_N$ as a tool for the study of K6 polyUb

To further characterize the activity of $LotA_N$ toward K6 polyUb, we constructed a fluorescent K6 diUb substrate (see STAR Methods) and monitored cleavage by fluorescence polarization (FP), as reported previously[41–43]. Through measuring initial rates of catalysis over a range of substrate concentrations, Michaelis-Menten parameters could be extracted for $LotA_N$ against K6 diUb (Fig. 2A, S2A). Despite a relatively high K_M, $LotA_N$ demonstrated an overall catalytic efficiency that is similar to other linkage-specific OTU DUBs, including the K11-specific Cezanne and the M1-specific OTULIN[42,44].

To further benchmark the utility of $LotA_N$ as a tool, we tested if specificity is retained even at high enzyme concentrations. Remarkably, even at very high (5 μM) enzyme concentration against both tetra- and longer polyUb samples, $LotA_N$ exclusively cleaved only K6 linkages (Fig. 2B–C, S2B). To test $LotA_N$'s utility in releasing K6 linkages from complex, heterogeneous mixtures, we tested it alongside other linkage-specific DUBs in several Ubiquitin Chain Restriction (UbiCRest) analyses[38,45,46].

The HECT-like E3 ligase NleL from enterohemorrhagic *Escherichia coli* has been reported to assemble mixed K6 and K48 polyUb chains[26,45]. Alongside the constitutively-activated K48-specific DUB OTUB1*[47], $LotA_N$ could indeed confirm this chain architecture in a UbiCRest assay. Treatment of NleL-assembled polyUb with either $LotA_N$ or OTUB1* resulted in a partial collapse of the polyUb smear down to shorter chains such as diUb, as well as a partial return of the monoUb band, while treatment with either the K11-specific Cezanne or the constitutively-activated K63-specific AMSH* had no effect (Fig. 2D)[47]. Co-incubation of the linkage-specific DUBs and comparison to the nonspecific vOTU revealed the abundance of K6 linkages present in the NleL assembly (Fig. 2D)[38,48].

As a further test, we generated polyUb chains with HUWE1, a human HECT E3 ligase that is reported to assemble a mixture of K6-, K11-, and K48-linked chains[13,21,49]. Treatment with Cezanne released the largest amount of monoUb, followed by OTUB1*, then $LotA_N$, and finally AMSH*, which had only a marginal amount of activity (Fig. 2E). DUB co-

incubation with or without $LotA_N$ showed a slight difference attributable to K6 linkages, especially at the level of released short polyUb products (Fig. 2E). Combined treatment of $LotA_N$, Cezanne, OTUB1*, and AMSH* hydrolyzed the assembled polyUb to a similar extent as vOTU, indicating that K11, K48, and K6 linkages form the bulk of HUWE1 products (Fig. 2E). Thus, the high level of activity and specificity exhibited by $LotA_N$ makes it a powerful tool that can be used alongside other linkage-specific enzymes to study K6 polyUb.

Structural analysis of $LotA_N$

The distinctive sequence and catalytic properties of $LotA_N$ warranted structural analysis for comparison to the other Lot DUBs. We determined a 1.5Å crystal structure of $LotA_N$ residues 1–294 using SAD phasing on bound iodide ions (Fig. 3A, S3A, Table 1). Overall, the $LotA_N$ structure resembled other Lot DUBs, with a papain-like OTU domain and a characteristic α-helical insertion domain at Variable Region 1 (VR-1), but additionally revealed several notable features (Fig. 3A). Firstly, the catalytic triad, comprised of C13, H237, and N239, was misaligned and beyond hydrogen bonding distance in the structure. In fact, two conformations of the C13 side chain were visible in the electron density, whereas no electron density was observed for the H237 imidazole ring (Fig. 3B). Despite this, mutation of C13, H237, and to a lesser extent N239 all severely decreased the ability of $LotA_N$ to cleave the fluorescent K6 diUb substrate (Fig. 3C).

The core OTU fold of $LotA_N$ closely resembles those of the other Lot-class DUBs (Fig. 3D), as well as the most closely related OTU DUBs from humans, viruses, and bacteria outside of *Legionella*[31–34,48,50–52] (Fig. S3B–D). At the putative S1 Ub-binding site, $LotA_N$ more closely follows the other Lot-class DUBs with a large helical domain inserted at VR-1, and minimal structural features at VR-2 and VR-3 compared to other OTU domains[32] (Fig. 3D, S3B–D). All of the Lot-class insertion domains structurally resolved thus far exhibit distinguishing adaptions of an underlying helical sub-structure and distinct orientations with respect to the OTU domains (Fig. 3D), a feature that has been proposed to contribute to the various polyUb specificities observed within this class of DUBs. A closer look at the catalytic triad across Lot-class DUBs reveals that, like $LotA_N$, the active site of $LotA_M$ is also misaligned in the observed crystal structure, whereas the active sites of LotB, LotC, and Ub-bound LotC are all in proper alignment for catalysis (Fig. 3E). This discrepancy in alignment is consistent with our observation that neither $LotA_N$ nor $LotA_M$ could cleave the monomeric Ub-KG(TAMRA) substrate (Fig. 1D), whereas LotB and the related LotD were previously shown to be active in the same assay[32]. This suggests that $LotA_N$ and $LotA_M$ are distinct from other Lot-class DUBs in their requirement for some form of substrate-assisted catalysis akin to that observed previously for the M1-specific DUB OTULIN[42].

Mechanism of K6 diUb recognition by $LotA_N$

To understand the molecular basis of $LotA_N$ activation and K6 polyUb specificity, we determined a 2.8Å crystal structure of $LotA_N$ in complex with K6 diUb by molecular replacement (Fig. 4A, S4A–B, Table 1). In the structure, K6 diUb is bound across the $LotA_N$ active site, sandwiched between the OTU core and the helical insertion domain (Fig. 4A). In order to preserve the K6 diUb while retaining binding to $LotA_N$, the active site

C13A mutation was used. Despite this, the electron density between the $LotA_N$-bound Ub molecules more closely supports a structural intermediate just after isopeptide cleavage, with no density connecting the ε-amino group of K6 from Ub^{prox} with the carbonyl carbon of G76 in Ub^{dist} (Fig. 4B). Rather than cleavage of the K6 linkage, we believe this lack of clear electron density is either due to a shift in register (i.e., Ub^{dist} and Ub^{prox} are bound into the S1' and S1 sites, respectively, of symmetry-related $LotA_N$ molecules) or symmetry averaging across related asymmetric units, as the C-terminus of Ub^{prox} is in close proximity to the K6 of a symmetry-related Ub^{dist} (Fig. S4C). The symmetry-related expansion of polyUb chains has been observed in other crystal structures[47], and in this case suggests that $LotA_N$ exhibits endo-DUB activity that can cleave anywhere within a polyUb chain. Although the catalytic C13 is mutated to alanine, the electron density clearly supports proper alignment and hydrogen bond distance of the remaining H237 and N239 triad members (Fig. 4B), indicating a structural rearrangement upon K6 diUb binding that will be discussed in more detail below.

In isolation of binding partners, crystallography and solution NMR data support a predominately closed conformation of K6 diUb, in which the Ub^{dist} I36 hydrophobic patch is bound to the Ub^{prox} I44 hydrophobic patch (Fig. 4C)[41,45]. In contrast, $LotA_N$ appears to select an open conformation of K6 diUb such that it can interact with the Ub^{dist} I36 patch as well as the I36 and F4 hydrophobic patches of Ub^{prox} (Fig. 4C). Selection among heterogeneous K6 diUb conformations appears to be an emerging trend of K6-interacting proteins, as distinct K6 diUb structures have been resolved in complexes with an engineered affimer protein, the DUB USP30, the NZF Ub-binding domain of TAB2, and now also $LotA_N$ (Fig. S4D)[13,16,53].

The interaction with Ub^{dist} at the $LotA_N$ S1 site appears to be mainly driven through an interface between the inserted helical domain at VR-1 and the I36 patch of Ub^{dist} (Fig. 4A, C). In contrast, the structure of LotC bound to Ub shows a stark ~180-degree rotation and a primary interface at a nonconserved VR-2 region (Fig. 4D). At the core of the interface, an extended loop region of the $LotA_N$ insertion domain slots L128 into a shallow pocket of Ub^{dist} formed between I36, L71, and T7 (Fig. 4E). Additional ionic interactions are observed around the periphery, including hydrogen bonds to both R72 and R74 of Ub^{dist} as the C-terminus enters the $LotA_N$ active site (Fig. 4E). This interface appears to play a minor role in the binding of K6 diUb, as an L128A mutation had minimal effect, and only a severe L128R mutation that introduces a steric clash with the Ub^{dist} I36 patch significantly disrupted $LotA_N$ cleavage of the fluorescent K6 diUb substrate (Fig. 4F).

The $LotA_N$ S1' site orients K6 of Ub^{prox} into the active site through interactions with the Ub I36 and F4 hydrophobic patches (Fig. 4A, C). The human DUB USP30 also recognizes the F4 patch of a K6-linked Ub^{prox}, but in a very different manner involving a ~100-degree twist (Fig. 4G, S4D). In the $LotA_N$ structure, Ub^{prox} is sandwiched between the core OTU and insertion domains and makes a single hydrogen bond to R74 of Ub^{dist} through the carbonyl oxygen of T9 (Fig. 4H). The F4 side chain of Ub^{prox} makes Van der Waals interactions to the peptide backbone of D10 within the $LotA_N$ OTU core domain (Fig. 4H). At the Ub^{prox} I36 patch, F120 and L141 from the $LotA_N$ insertion domain interact with I36, while buried within the interface lies a salt bridge between $LotA_N$ R145 and Ub^{prox} E34. Mutation

of these residues in $LotA_N$ had a much more severe impact on K6 diUb cleavage than mutations in the S1 site (Fig. 4F,I). Reciprocal mutations specifically introduced into Ub^{prox} of K6 diUb (see STAR Methods) showed the strongest cleavage defect with mutation of F4, a modest effect with I36 mutation, and no effect upon mutation of the unutilized I44 site (Fig. 4J).

The $LotA_N$ insertion domain makes key contributions to both the S1 and S1' Ub-binding sites required for DUB activity. Despite their differences, the core structures of the Lot-class insertion domains follow a related underlying 4-helix topology (Fig. 4K, S4E). By structural comparison using Dali[52], the insertion domain of $LotA_N$ is the most similar to LotC over other Lot-class DUBs (Fig. S4F). Based on the Ub- and diUb-bound structures of LotC and $LotA_N$, respectively, it is the distinguishing features of the α1–2 region that dictate interactions to Ub (Fig. S4F–H)[34]. Modeling and mutagenesis studies implicate the α1–2 regions of LotB and $LotA_M$ in mediating important Ub interactions as well[33,50]. Interestingly, Dali searches also detected similarity to the VR-1 region of OtDUB, an effector DUB from *Orientia tsutsugamushi* that belongs to the CE clan of cysteine proteases[54] (Fig. S4I). The OtDUB VR-1 region follows the 4-helix structural topology conserved among Lot-class DUBs, and encodes two Ub-binding sites: one at the edge of Helix 3 that forms part of the S1 site to bind Ub^{dist} (Fig. S4J), and a second located in the α1–2 region that binds an additional Ub with unusually high affinity (Fig. S4K). Unlike the high affinity site in the α1–2 region (Fig. S4K), residues at the edge of Helix 3 in OtDUB VR-1 are conserved in the $LotA_N$ structure (Fig. S4J). Additional binding of Ub at this site in $LotA_N$, however, would cause steric clash with the Ub^{dist} observed in our structure (Fig. S4J). Because of its important roles in Lot-class DUBs as well as OtDUB, we propose to assign the name Adaptive Ubiquitin-Binding Domain, or "A-UBD" for short, to this common 4-helix substructure, owing to adaptations of the α1–2 regions that impart distinctive Ub interactions into a common topological scaffold (Fig. 4K, S4E).

Conformational changes leading to $LotA_N$ activation

Comparison of the apo and K6 diUb-bound $LotA_N$ structures revealed several interesting changes. First, the complex structure exhibited a 45-degree swing of the A-UBD with respect to the core OTU domain, resulting in a more closed conformation (Fig. 5A). This swing moves key residues such as L128, F120, and R145 up, forming the S1 and S1' Ub-binding sites that sandwich K6 diUb against the active site (Fig. 5B, 4E, 4H). Movement within the hinge region is required for $LotA_N$ activity, as a stabilizing A193P hinge mutation reduces cleavage of the fluorescent K6 diUb substrate, while an A193G mutation retains the mobility required for function (Fig. 5C). Analogous hinge regions can be observed between the core OTU and A-UBDs of other Lot-class DUBs (Fig. S5). Comparison of the apo and Ub-bound LotC structures shows a 6-degree swing, in this case toward a more open conformation in the Ub-bound complex (Fig. S5). Thus, it is possible that other Lot-class DUBs may also require mobility of the A-UBD for DUB activity.

Another dramatic difference between structures is in the active site. As highlighted above, the $LotA_N$ catalytic triad is misaligned in the apo structure but properly aligned for catalysis in the diUb-bound structure (Fig. 3B and 4B). Coincident with this rearrangement, the

so-called “Cys loop” preceding the catalytic cysteine is shifted by >4Å toward the remaining triad members. Opposing the Cys loop is F4 of Ub^{prox}, which appears to select for this active conformation by creating steric conflict with the conformation observed in the apo structure (Fig. 5D). This contact is critical for $LotA_N$ activation, as K6 diUb incorporating a Ub^{prox} F4A mutation cannot be cleaved (Fig. 4J). The so-called “His loop” preceding the general base histidine is also shifted by >3Å between structures (Fig. 5D). Opposing this loop is H68 of Ub^{prox}, which makes a hydrogen bond to the backbone carbonyl of E235 in the complex structure (Fig. 5D). This interaction is also important for $LotA_N$ activation, as K6 diUb incorporating a Ub^{prox} H68A mutation is cleaved less efficiently than wild-type (Fig. 5E). This function of Ub^{prox} H68 relies on both hydrogen bonding and steric effects, as Ub^{prox} H68Q or H68F mutants are also cleaved less efficiently (Fig. 5E). Thus, Ub binding at the S1’ site in the correct, K6-specific orientation activates the $LotA_N$ catalytic center through substrate-assisted catalysis, by which F4 and H68 of Ub^{prox} assist in the proper orientation of the Cys and His loops.

A mechanism of substrate-assisted catalysis is consistent with the observed lack of activity against the monomeric Ub-KG(TAMRA) substrate (Fig. 1D), wherein Ub would presumably bind at the S1 site but the attached KG(TAMRA) moiety occupying the S1’ site could not serve to activate the catalytic triad. $LotA_N$ can, however, react with the monomeric Ub-PA activity-based probe (Fig. 1C). As expected, the Ub-PA reactivity observed in wild-type $LotA_N$ is abolished or severely reduced in the backgrounds of the catalytic C13A or S1-site L128R mutations, respectively (Fig. 5F). Unexpectedly, reactivity was also lost in the S1’-site R145L and the hinge A193P mutants (Fig. 5F). To test if one molecule of Ub-PA is binding at the S1’ site to activate reactivity for a second, we generated an F4A mutant to block any role in activation (see Fig. 4J and 5D). Compared to wild-type Ub-PA, reactivity of the F4A mutant is severely reduced (Fig. 5G). Addition of wild-type but not F4A Ub (lacking the PA warhead) rescues reactivity of F4A Ub-PA by serving as a dedicated “activator” for substrate-assisted catalysis at the S1’ site (Fig. 5G). A prerequisite of substrate-assisted catalysis is movement of the $LotA_N$ A-UBD, as the A193P hinge mutant overrides all Ub-PA reactivity (Fig. 5G).

$LotA_N$ activity is required for restriction of K6 polyUb at the *Legionella*-containing vacuole

LotA, LotB, and LotC have all been shown to edit Ub modifications deposited onto the LCV[30,31,34]. LotA regulates K6, K48, and K63 polyUb following localization via its C-terminal PI(3)P-binding domain[30] (Fig. 1A). Whether these signal types are independently regulated by LotA’s two OTU domains, however, had not been tested. We constructed *L. pneumophila* strains with genomic *lotA* mutations at either OTU active site (C13S, C303S) for comparison to the wild-type Lp01 and Δ*lotA* strains, and performed infections in HeLa-FcγRII cells expressing a reporter for K6 polyUb (see STAR Methods). Compared to the wild-type strain, deletion of *lotA* results in a significant increase in the number of K6-positive LCVs (Fig. 6A–B). While the $LotA_M$ C303S mutant restricts K6 polyUb like wild-type, the $LotA_N$ C13S mutant phenocopies *lotA* deletion (Fig. 6A–B). These findings are consistent with our *in vitro* specificity analyses (Fig. 1E–H), and suggest a delineation of roles during infection.

As a further test of our structure-guided mechanistic studies, we designed two separate triple-mutant variants of $LotA_N$: “FRA” combines S1’-site F120A and R145L with the hinge A193P mutation, while “LRA” combines S1-site L128R, S1’-site R145L, and hinge A193P mutations. *In vitro*, neither variant could cleave K6 diUb, even at high concentration (Fig. S6A). *L. pneumophila* strains carrying either *lotA* triple-mutant variant failed to restrict K6 polyUb (Fig. 6C, S6B), demonstrating that the requirements for $LotA_N$ activity *in vitro* hold true during infection.

The importance of LotA DUB activities for *L. pneumophila* growth was tested by infecting mouse bone marrow-derived macrophages (BMDMs) with the various mutagenized stains. As reported previously[30], deletion of *lotA* resulted in no significant defect in *L. pneumophila* intracellular growth in BMDMs, whereas a secretion-deficient Δ*dotA* strain failed to replicate (Fig. 6D). Strains carrying integrated catalytic mutations in either $LotA_N$ (C13S) or $LotA_M$ (C303S) behaved like wild-type and Δ*lotA L. pneumophila*, with no apparent growth phenotype (Fig. 6D).

One proposed signaling role for K6 polyUb is as a preferred target for the AAA ATPase VCP/p97/Cdc48, which extracts ubiquitinated targets for degradation. We examined VCP localization following infection with our mutagenized *L. pneumophila* strains. Infection with wild-type *L. pneumophila* resulted in low but significant VCP recruitment to the LCV compared with a secretion-deficient Δ*dotA* strain, as previously observed[55] (Fig. 6E–F, S6C). Loss of DUB activity through *lotA* deletion or double C13S C303S mutation starkly increased VCP recruitment (Fig. 6E–F, S6C). Individual $LotA_N$ and $LotA_M$ active site mutants both exhibited significantly more VCP recruitment than wild-type *L. pneumophila*, indicating nonredundant roles (Fig. 6E–F, S6C). These findings are consistent with a role for K6-, as well as potentially K48- and K63-linked polyUb, in recruiting VCP to the LCV during infection.

DISCUSSION

The identification of K6-specific enzymes in humans has proven difficult[10,13,16,38,56]. Meanwhile, the first OTU domain of *L. pneumophila* LotA is extremely specific and highly active toward K6 polyUb. Perhaps coincidentally, the most K6-specific E3 ligase identified to date, NleL, also originates from bacteria[26]. Just as NleL has become an invaluable tool for studying K6 polyUb[45], $LotA_N$ will be equally useful, particularly in applications such as UbiCRest analyses. Prior use of OTUD3 as a K6-targeted DUB has required careful consideration of enzyme concentration and secondary activities[46]. We show that $LotA_N$ maintains K6 specificity even at high concentration against long, complex polyUb chains, and will thus be a convenient tool alongside other polyUb-specific DUBs.

The exquisite specificity of $LotA_N$ toward K6 polyUb arises from a blend of regulatory mechanisms (Fig. 7). In our apo structure of $LotA_N$, the open conformation of the A-UBD is incompatible with polyUb binding and the active site is misaligned. Consistent with inherent flexibility in these regions, the $LotA_N$ Cys loop, His loop, and hinge region all exhibit above average B-factors. Before polyUb binding can occur, flexibility is required in the $LotA_N$ hinge for the A-UBD to swing into position. This *in situ* formation of Ub-binding sites

resembles the human DUB Cezanne binding to K11 diUb[44]. In addition, only binding of a K6-linked Ub^{prox} would select for the catalytically-competent alignment of the Cys and His loops. The human DUB OTULIN uses a similar mechanism of substrate-assisted catalysis to ensure M1 polyUb specificity[42]. Unlike LotB and LotC, $LotA_M$ also appears to require some form of substrate-assisted catalysis for active site rearrangement, in addition to its requirement for longer polyUb chains.

Helical sub-domains inserted into VR-1 of the OTU domain are a defining feature of Lot-class DUBs. While the basic ~4-helix fold is similar, adaptations to the α1–2 region add versatility to the Ub interface, hence our proposed name Adaptive Ubiquitin-Binding Domain, or "A-UBD" (Fig. 4K, S4E). The A-UBD α1–2 regions of $LotA_N$, $LotA_M$, LotB, LotC, as well as OtDUB all play important roles in mediating Ub interactions[33,34,50,54]. It is remarkable that this domain, now observed in at least 5 cases across two bacterial species, has adopted such distinct Ub interactions. To what extent the A-UBD is incorporated into other regulators of Ub signaling across bacteria, viruses, and eukaryotes will be an interesting area of future research.

During infection, $LotA_N$ and $LotA_M$ regulate distinct polyUb signals on the LCV surface (Fig. 7). The close spacing of the two OTU domains (~20 amino acids), however, raises the interesting possibility that they work cooperatively on a large or particularly complex polyUb signal. Though no apparent growth phenotype was observed for the C13S mutant within $LotA_N$, functional redundancies among the ~300 secreted *L. pneumophila* effectors often mask phenotypic differences in single-mutant strains. The DUB activity of $LotA_M$ was previously shown to genetically interact with the SidE family of secreted E3 Ub ligases[30]. Whether the K6-specific activity of $LotA_N$ functions in concert with other secreted effectors remains to be seen. LotA's two DUB activities play nonredundant roles in preventing recruitment of the AAA ATPase VCP/p97/Cdc48 to the LCV. Thus, one possible evolutionary rationale for LotA's two OTU domains with distinct activities and specificities is that they guard different subsets of proteins on the LCV from VCP-dependent extraction and proteasomal degradation. K6 polyUb signals have also been previously tied to the autophagic destruction of mitochondria and bacteria by the E3 ligase Parkin[8,57], raising the possibility that LotA acts together with other *L. pneumophila* effectors to restrict host autophagic defenses[58]. Whether and how $LotA_N$ might fit into this or other K6 signaling networks, and what additional facets of K6 polyUb biology might be uncovered as a result, will be an exciting area of future work.

Limitations of the study

While we could reliably demonstrate the exquisite specificity of $LotA_N$, even at high enzyme concentration against long polyUb chains, we cannot predict how additional complications such as Ub acetylation or phosphorylation might impact $LotA_N$'s activity or specificity. Furthermore, our testing of $LotA_N$ in UbiCRest analyses of complex, heterotypic, and branched polyUb chains was limited to the few Ub conjugation systems known to assemble K6 linkages. Future applications of $LotA_N$ to the study of K6 polyUb will build upon this foundation and establish its reliability as a steadfast research tool.

Studying the role of LotA's K6 specificity during infection is limited by several parameters. Firstly, the lack of a readily available detection reagent for K6 polyUb necessitated the expression of the exogeneous HA-Ub-K6 construct. While we are confident that HA-Ub-K6 is a reliable reporter of K6 polyUb in this case (owing to the strict specificity of $LotA_N$), expression levels could influence the amount of K6 polyUb we observe. Our ability to assess the relevance of K6-specific DUB activity on *L. pneumophila* growth was also hindered by redundancies among the ~300 secreted effectors. The importance of LotA activity could also be more apparent in a different host organism, such as amoebae or ciliated protozoa. Regardless, our findings indicate that the study of LotA in mammalian cells will still yield new insights into the signaling roles for this atypical linkage type.

STAR METHODS

Resource availability

Lead contact—Further information and requests for resources and reagents should be directed to and will be fulfilled by the lead contact, Jonathan N. Pruneda (pruneda@ohsu.edu).

Materials availability—All reagents generated from this study are available from the lead contact upon request.

Data and code availability

- Coordinates and structure factors for the apo and K6 diUb-bound $LotA_N$ structures have been deposited in the Protein Data Bank under accession codes 7UYG and 7UYH, respectively, and will be publicly available as of the date of publication.
- This paper does not report original code.
- Any additional information required to reanalyze the data reported in this paper is available from the lead contact upon request.

Experimental model and subject details

TOP10 *Escherichia coli* (ThermoFisher) were used for all cloning and plasmid propagation. Rosetta (DE3) *E. coli* (MilliporeSigma) were used for all recombinant protein expression. DH5αλpir *E. coli* (BEI Resources) were used for allelic exchange. All *E. coli* strains were grown at 37°C in Luria-Bertani (LB) media containing appropriate antibiotics.

Legionella pneumophila Philadelphia-1 (Lp01) were used as the wild-type strain in our studies[69]. All mutations were introduced into the base *L. pneumophila* strain by allelic exchange and confirmed by PCR and DNA sequencing[70]. Luciferase-expressing strains were constructed as described previously[71]. All *L. pneumophila* strains were grown at 37°C in liquid N-(2-acetamido)-2-aminoethanesulfonic acid (ACES; MilliporeSigma)-buffered yeast extract (AYE) media or on charcoal-yeast extract (CYE) plates, as described previously[72].

HeLa-FcγRII cells (a kind gift from K. Arasaki at Tokyo University of Pharmacy and Life Sciences) were grown in Minimum Essential Medium α (MEMα; Gibco) supplemented with 10% fetal bovine serum (FBS) and 400 μg/mL hygromycin (Nacarai)[59].

Murine bone marrow-derived macrophages were prepared from A/J mice (A/JJmsSlc; Japan SLC) and maintained in RPMI 1640 Medium (GIBCO) supplemented with 5% L cell supernatant and 10% FBS as described previously[60].

Method details

Cloning and mutagenesis—The *lotA* gene was cloned from *Legionella pneumophila* Philadelphia-1 genomic DNA. Initial construct design was performed using Phyre2[73] and the $LotA_M$ crystal structure[50], yielding construct boundaries of 1–300 and 287–543 for $LotA_N$ and $LotA_M$, respectively. To support crystallization, additional C-terminal truncations of $LotA_N$ led to the 1–294 construct used for determination of the apo $LotA_N$ structure. Based on the apo structure, an additional $LotA_N$ construct encoding amino acids 1–276 was used for determination of the K6 diUb-bound structure. All LotA constructs were cloned into the pOPINB vector, which encodes an N-terminal His tag followed by a 3C protease cleavage site. Cloning and mutagenesis were performed using Phusion DNA Polymerase (New England BioLabs) and TOP10 *E. coli* (ThermoFisher).

Protein expression and purification—All pOPINB-LotA constructs were expressed and purified similarly. Transformed Rosetta (DE3) *E. coli* were grown in Luria broth containing 35 μg/mL chloramphenicol and 50 μg/mL kanamycin at 37°C until an optical density (600 nm) of 0.6–0.8. Cultures were cooled to 18°C and induced with 0.2 mM IPTG for an additional 20 hours. Cells were harvested by centrifugation and resuspended in 25 mM Tris, 200 mM NaCl, 2 mM β-mercaptoethanol, pH 8.0 (Buffer A). Following a freeze-thaw cycle, cells were incubated on ice with lysozyme, DNase, and SigmaFAST protease inhibitor cocktail (MilliporeSigma) prior to lysis by sonication. Clarified lysates were applied to HisPur cobalt affinity resin (ThermoFisher) and washed with Buffer A prior to elution with Buffer A containing 300 mM imidazole. Eluted proteins were cleaved with 3C protease overnight during dialysis back to Buffer A at 4°C. Cleaved LotA proteins were concentrated using 10K MWCO Amicon centrifugal filters (MilliporeSigma) and applied to a HiLoad Superdex 75 pg size exclusion chromatography column (Cytiva) equilibrated in 25 mM Tris, 200 mM NaCl, 5 mM DTT, pH 8.0. Fractions were evaluated for purity by SDS PAGE, collected, concentrated, and quantified by absorbance (280 nm) prior to flash freezing and storage at −80°C.

Untagged Ub constructs were expressed from the pET-17b vector. Transformed Rosetta (DE3) *Escherichia coli* were grown by auto-induction in a modified ZYM-5052 media[74] containing 35 μg/mL chloramphenicol and 100 μg/mL ampicillin at 37°C for 24–48 h. Cells were harvested by centrifugation, resuspended, and lysed as above for LotA. Clarified lysates were acidified by dropwise addition of 70% perchloric acid to a final concentration of 0.5%. The mixture was allowed to stir on ice for 1–2 h prior to centrifugation. The supernatant was dialyzed against 50 mM sodium acetate, pH 4.5 overnight at 4°C. The protein was applied to a HiPrep SP FF 16/10 cation exchange column (Cytiva), washed

with additional 50 mM sodium acetate, pH 4.5, and eluted over a linear gradient to a matched buffer containing 500 mM NaCl. Fractions were evaluated for purity by SDS PAGE, pooled, and dialyzed against 25 mM Tris, 200 mM NaCl, pH 8.0 overnight at 4°C. If necessary, further purification was performed using a HiLoad Superdex 75 pg size exclusion chromatography column (Cytiva) equilibrated in 25 mM Tris, 200 mM NaCl, pH 8.0. Purified Ub was concentrated using 3K MWCO Amicon centrifugal filters (MilliporeSigma), quantified by absorbance (280 nm), and flash frozen for storage at either −20°C or −80°C.

The Ub-PA activity-based probes were prepared using intein chemistry as described previously[75]. Rosetta (DE3) *Escherichia coli* transformed with pTXB1-Ub(1–75) were grown in Luria broth containing 35 μg/mL chloramphenicol and 100 μg/mL ampicillin at 37°C until an optical density (600 nm) of 0.6–0.8. Cultures were cooled to 18°C and induced with 0.5 mM IPTG for an additional 20 hours. Cells were harvested by centrifugation and resuspended in 20 mM HEPES, 50 mM sodium acetate, 75 mM NaCl, pH 6.5 (Buffer B). After a freeze-thaw cycle, cells were incubated on ice with DNase, SigmaFAST protease inhibitor cocktail (MilliporeSigma), and PMSF prior to lysis by sonication. The clarified lysate was applied to chitin resin (New England BioLabs) and allowed to bind at 37°C for 2 h. The resin was washed with Buffer B, followed by a high salt wash with Buffer B containing 500 mM NaCl, followed by a final wash with Buffer B. The Ub-MesNa was allowed to form and elute from the chitin resin for 42 h at room temperature, following addition of Buffer B containing 100 mM MesNa. The eluted protein was concentrated using 3K MWCO Amicon centrifugal filters (MilliporeSigma) and applied to a HiLoad Superdex 75 pg size exclusion chromatography column (Cytiva) equilibrated in Buffer B. Fractions containing Ub-MesNa were evaluated for purity by SDS PAGE and pooled. To convert Ub-MesNa to Ub-PA, propargylamine hydrochloride was added in 1000-fold excess and, following adjustment of the pH to 8.5, incubated at room temperature for 3 h. The reaction was dialyzed against 25 mM Tris, 200 mM NaCl, pH 8.0 overnight at 4°C. The final product was concentrated using 3K MWCO Amicon centrifugal filters (MilliporeSigma), quantified by absorbance (280 nm), and stored on ice during immediate use.

Assembly of polyUb chains—All diUb and tetraUb chains were assembled and purified according to published methods[76], with the exception of K27 diUb and K11 tetraUb, which were purchased from UbiQ and R&D Systems, respectively. K6 diUb for fluorescent labeling or for experiments that incorporate Ub^{prox} mutations were assembled using a "capped" strategy that allows directed formation of K6-linked diUb from dedicated donor and acceptor Ub moieties that are incorporated as Ub^{dist} and Ub^{prox}, respectively. The dedicated donor Ub construct incorporated K6R and K48R mutations, but retained an intact C-terminus. The dedicated acceptor Ub construct incorporated a K48R mutation and lacked the C-terminal LRGG motif. Effects of Ub^{prox} mutation were assessed by incorporating additional mutations into the dedicated acceptor Ub construct. Alternatively, a Ub^{prox} for fluorophore labeling was incorporated with an acceptor Ub construct that coupled a deletion of G76 with a G75C mutation. Equimolar amounts of donor and acceptor Ub variants were combined with 100 nM UBE1, 600 nM UBE2L3, 10 μM NleL, and 10 mM ATP in buffer containing 40 mM Tris, 10 mM $MgCl_2$, 0.5 mM DTT, pH 8.5. Reactions were incubated

at 37°C for 16 h and subsequently quenched by addition of 10 mM DTT and 50-fold dilution into 50 mM sodium acetate, pH 4.5. The reactions were applied to a HiPrep SP FF 16/10 cation exchange column (Cytiva), washed with additional 50 mM sodium acetate, pH 4.5, and eluted over a linear gradient to a matched buffer containing 500 mM NaCl. Fractions were evaluated for purity by SDS PAGE, pooled, and dialyzed against 25 mM Tris, 200 mM NaCl, pH 8.0 overnight at 4°C. The diUb product was concentrated using 3K MWCO Amicon centrifugal filters (MilliporeSigma), quantified by absorbance (280 nm), flash frozen, and stored at either −20°C or −80°C.

Fluorescent K6 diUb was prepared using the “capped” strategy described above, which allows specific labeling of a cysteine incorporated at position 75 of Ub^{prox}. Purified K6 diUb was diluted to 50 μM in 25 mM sodium phosphate, 150 mM NaCl, 10 mM DTT, pH 7.4 and incubated at room temperature for 30 min. The diUb was subsequently buffer exchanged into 25 mM sodium phosphate, 150 mM NaCl, pH 7.4 over a PD-10 desalting column (Cytiva). ATTO488-maleimide (ATTO-TEC) was added in 5-fold molar excess to 1 mL of the desalted K6 diUb, and incubated at room temperature in the dark for 18 h. The labeled K6 diUb was again desalted to remove excess fluorophore, quantified by absorbance (488 nm), and flash frozen for storage at −80°C.

Gel-based DUB assays—Gel-based DUB assays were performed according to published methods[77]. DUBs were prepared at 2X concentration in 25 mM Tris, 150 mM NaCl, 10 mM DTT, pH 7.4 and incubated at room temperature for 10 min. Equal volumes of 2X DUB and either 10 μM diUb or 5 μM tetraUb were mixed and incubated at 37°C. Samples were quenched in Laemmli sample buffer containing 0.2 M dithiothreitol (DTT) and analyzed by SDS PAGE.

Ub-PA reactivity assays—Ub-PA reactivity assays were performed according to published methods[77]. DUBs were diluted to 10 μM in 25 mM Tris, 150 mM NaCl, 10 mM DTT, pH 7.4 and incubated at room temperature for 10 min. Equal volumes of 2X DUB and 100 μM Ub-PA were mixed and allowed to react at room temperature for up to 18 h, prior to being quenched in Laemmli sample buffer containing 0.2 M DTT and analyzed by SDS PAGE. For rescue experiments with the F4A Ub-PA variant, 25 μM wild-type or F4A Ub was added to the above reaction.

Fluorescence-based DUB assays—Ub- and Ubl-KG(TAMRA) substrates were prepared as previously described[37,78]. Cleavage of the Ub- and Ubl-KG(TAMRA) substrates was monitored by fluorescence polarization according to published methods[77]. Enzymes and substrates were prepared at 2X concentration in 25 mM Tris, 100 mM NaCl, 5 mM β-mercaptoethanol, 0.1 mg/mL BSA, pH 7.4 and mixed 1:1 to initiate the reaction. All substrates were held at 50 nM concentration, while protease concentrations were adjusted according to their specific activities. Fluorescence polarization was recorded using a BMG LabTech ClarioStar plate reader with an excitation wavelength of 540 nm, an LP 566 nm dichroic mirror, and an emission wavelength of 590 nm. Reactions were performed in Greiner 384-well small-volume HiBase microplates with 20 μL reaction volumes. Three technical replicates were performed for each reaction, with additional wells containing KG(TAMRA) and Ub/Ubl-KG(TAMRA) as positive and negative controls, respectively.

Fluorescence polarization was recorded once per minute over a 1–2 h time period. Data collected from the positive and negative control wells were used to convert fluorescence polarization measurements to fraction of substrate remaining.

DUB assays using the ATTO488-labeled K6 diUb substrate were performed as above, with minor changes. Fluorescence polarization was monitored using an excitation wavelength of 482 nm, an LP 504 nm dichroic mirror, and an emission wavelength of 530 nm. Assay concentrations were 10 nM $LotA_N$ and 50 nM ATTO488-labeled K6 diUb, except for the $LotA_N$ triple-mutants, which were also assayed at a higher enzyme concentration of 1 μM. ATTO488-labeled monoUb and diUb were used as positive and negative controls, respectively, and used to convert fluorescence polarization measurements to fraction of substrate remaining. To determine Michaelis-Menten parameters, $LotA_N$ concentration was held at 4 nM and initial rates of cleavage were determined from the linear range of data produced over the first 15–25 minutes of the reaction, across a range of substrate concentrations from 100 nM to 50.1 μM. All substrate concentrations maintained a fixed, 100 nM concentration of ATTO488-labeled K6 diUb, while unlabeled K6 diUb (shown to be hydrolyzed equally well) was used for the remainder. Three technical replicates were performed for each reaction, and three separate trials were performed for each K6 diUb concentration. Positive and negative control measurements were used to convert fluorescence polarization data to amount of substrate consumed, which was used to derive initial rates. Prism 9 was used for Michaelis-Menten analysis of the initial rate data.

UbiCRest analysis—Linkage-specific polyUb chains were assembled according to published methods[76]. NleL and HUWE1 chain assemblies were performed at 37°C for 2 h in 25 mM Tris, 150 mM NaCl, 10 mM $MgCl_2$, 0.5 mM DTT, pH 7.4 using 375 nM UBE1, 1.5 μM Lys-less UBE2L3, 5 mM ATP, and either 3.75 μM NleL (aa 170–782) or 15 μM HUWE1 (aa 3993–4373). Prior to DUB treatment, all polyUb assembly reactions were quenched by addition of 50 mM EDTA and 5 mM DTT. DUBs were diluted to 10 μM in 25 mM Tris, 150 mM NaCl, 10 mM DTT, pH 7.4 and incubated at room temperature for 10 min. Equal volumes of polyUb assembly and DUB were mixed and incubated at 37°C for 2 h, prior to quenching in Laemmli sample buffer containing 0.2 M DTT. Reactions were resolved by SDS PAGE prior to transfer onto PVDF membranes using a Trans-Blot Turbo system (BioRad). Membranes were blocked at room temperature for 30 minutes with TBS-T (Tris-buffered Saline containing 0.1% Tween-20) containing 5% milk, then incubated with primary anti-Ub antibody (MilliporeSigma, MAB1510-I; 1:1,000 dilution) at 4°C overnight. Membranes were washed in TBS-T and incubated with secondary antibody (MilliporeSigma, #12–349; 1:5,000 dilution) at room temperature for 1 hour before performing additional TBS-T washes and detection using Clarity ECL reagent (BioRad).

Protein crystallization and structure determination—$LotA_N$ (1–294), $LotA_N$ (1–276), and K6 diUb were prepared as described above and exchanged into 25 mM Tris, 125 mM NaCl, 5 mM DTT, pH 7.4. $LotA_N$ (1–294) was concentrated to 12 mg/mL and crystallized in hanging drop format with 30% PEG 2K MME, 0.2 M KI, 0.1 M MES pH 6.5 at 20°C in a 1 μL drop with 1:1 protein:precipitant ratio. $LotA_N$ (1–276) was mixed with an equimolar amount of K6 diUb and concentrated using a 3K MWCO Amicon

centrifugal filter (MilliporeSigma) to a total protein concentration of 8 mg/mL (determined by Bradford Assay). The protein complex was crystallized in hanging drop format with 25% PEG 3350, 10% ethylene glycol, 0.2 M KSCN, 0.1 M MES pH 5.5 at 20°C in a 1 μL drop with 1:1 protein:precipitant ratio. Apo $LotA_N$ crystals were cryoprotected in mother liquor containing 12.5% glycerol, while complex $LotA_N$ crystals were cryoprotected in mother liquor containing 25% glycerol prior to vitrification.

Diffraction data were collected at the Stanford Synchrotron Radiation Lightsource (SSRL), beamline 9–2. Images were integrated using XDS[61] and scaled using Aimless[63]. The apo $LotA_N$ (1–294) structure was determined by SAD using the SHELXC/D/E pipeline in CCP4i2[62,64], based on anomalous signal arising from bound iodide ions that were present in the crystallization condition. Automated model building was performed using ARP/wARP[65], followed by iterative rounds of manual model building in COOT and refinement in PHENIX[67,68]. Residues 2–275 could be confidently modeled into the electron density. The complex $LotA_N$ (1–276) structure bound to K6 diUb was determined by molecular replacement with Phaser in CCP4i2, using the apo $LotA_N$ and Ub (PDB 1UBQ) structures[62,66,79]. Model building and refinement were performed as above using COOT and PHENIX[67,68]. All figures were generated using PyMOL (www.pymol.org).

Legionella strains and culture—*L. pneumophila* strains used in this study are listed in Table S1. Point mutations in genomic *lotA* were introduced by a gene knock-in method, whereby mutated *lotA* genes were integrated into the Δ*lotA* strain at the endogenous locus[30]. Plasmids used for the integration were constructed based on pSR47S-Δ*lotA*[30], which contains homologous regions upstream and downstream of the endogenous *lotA* locus inserted into the pSR47S gene-replacement vector as follows[80]. The linearized pSR47S-Δ*lotA* was generated by PCR using primers lpg2248KI-1 and lpg2248KI-2. Fragments of the mutated *lotA* genes were obtained by PCR using primers lpg2248KI-3 and lpg2248KI-4 from pMMB207–3xFLAG-LotA C13S[30], 3xFLAG-LotA C303S[30], 3xFLAG-LotA C13S/C303S[30], pOPINB-LotA F120A/R145L/A193P, and pOPINB-LotA L128R/R145L/A193P. The vector and *lotA* fragments were ligated using Gibson assembly, and the resulting plasmids were transformed into *E. coli* DH5αλpir. The allelic exchange was conducted as described previously[70]. The genomic mutations of *lotA* were validated by PCR and subsequent DNA sequencing. The *L. pneumophila* strains were grown at 37°C in liquid N-(2-acetamido)-2-aminoethanesulfonic acid (ACES; MilliporeSigma)-buffered yeast extract (AYE) media or on charcoal-yeast extract (CYE) plates, as described previously[72].

Transfection and infection—HeLa-FcγRII cells were seeded on cover slips in 24-well tissue culture plates at 5×10^4 cells per well 24 h before transfection. If necessary, transfection was performed using Lipofectamine2000 (Invitrogen) and 500 ng of pRK5-HA-Ub-K6 (Addgene, #22900) for 24 h according to the manufacturer's recommendation. Because of the lysine-to-arginine mutations and the encoded N-terminal epitope tag, HA-Ub-K6 can only be utilized for a) monoubiquitination, b) as a distal capping Ub on the end of a polyUb chain, or c) incorporation into a K6-linked chain. Owing to its stringent requirement for substrate-assisted catalysis, $LotA_N$ would only be able to hydrolyze HA-Ub-K6 that is incorporated into K6-linked chains. For infection, *L. pneumophila* was cultivated

for 24 h in AYE media (with starting A_{600} of 0.2) at 37°C with shaking. The cells were infected with the *Legionella* strains opsonized with anti-*Legionella* rat antibody (Scrum, #17457; 1:3,000 dilution) or with anti-*Legionella* rabbit antibody (BioAcademia, #64–100; 1:3,000 dilution) at a multiplicity of infection (MOI) of 2. After adding bacteria to the cells, the plates were centrifuged at 200 × g to precipitate bacteria onto the layer of cells and were immediately warmed in a 37°C water-bath by floating for 5 min and then placed in a CO_2 incubator at 37°C. At 1 h after infection, the infected cells were washed three times with prewarmed Dulbecco's Phosphate Buffered Saline (DPBS; MilliporeSigma) to remove the extracellular bacteria and refreshed with prewarmed media, then incubation was resumed at 37°C in a CO_2 incubator. At 4 h after infection, the cells were washed three times with DPBS and fixed with 4% (w/v) paraformaldehyde for 20 min.

Immunofluorescent microscopy—For detection of HA-Ub-K6, the fixed HeLa-FcγRII cells on coverslips were permeabilized by treating with cold methanol for 60 sec and washed three times with DPBS. The samples were blocked with 2% (v/v) goat serum in DPBS and treated with anti-HA rabbit antibody (MBL, #561) with 1:200 dilution for 90 min. After three times washing with DPBS, the samples were treated with anti-*Legionella* rat antibody (Scrum, #17457; 1:3,000 dilution) for 60 min. After three times washing with DPBS, the samples were treated with secondary fluorescent antibodies, Alexa 488 goat anti-rabbit IgG (Invitrogen, #A11034; 1:500 dilution) and Alexa 568 goat anti-rat IgG (Invitrogen, #A11077; 1:500 dilution), for 40 min. After washing three times with DPBS, the coverslips were rinsed with distilled water and mounted on glass slides with ProLong™ Diamond Antifade Mountant with DAPI (Invitrogen, P36962). For detection of VCP, the fixed HeLa-FcγRII cells on coverslips were permeabilized and blocked by treating with 0.2% (v/v) Triton X-100 and 2% (v/v) goat serum in DPBS for 20 min. After washing three times in DPBS, the samples were then treated with anti-VCP mouse antibody (Abcam, #ab11433; 1:200 dilution) for 90 min, followed by treatment with anti-*Legionella* antibody (BioAcademia, #64–100; 1:3,000 dilution) for 60 min. After three additional washes in DPBS, the samples were treated with secondary fluorescent antibodies, Alexa488 goat anti-mouse IgG (Invitrogen, #A411029; 1:500 dilution) and RhodamineRedX anti-rabbit IgG (Invitrogen, #R6394; 1:1,000 dilution), for 40 min. After three final washes in DPBS, the coverslips were rinsed with distilled water and mounted on glass slides with ProLong™ Diamond Antifade Mountant with DAPI (Invitrogen, P36962). Images were collected with an inverted microscope (TE2000-U; Nikon) equipped with a digital ORCA-ERA camera (Hamamatsu). Images were blinded and quantified by manual counting of immunostained LCVs. In the case of experiments involving HA-Ub-K6, only LCVs contained within cells expressing the HA-Ub-K6 construct were used for counting.

Legionella intracellular growth assay—The luminescent *L. pneumophila* growth assay was conducted as described previously[30]. Mouse BMDMs (4×10^4 cells per well) were prepared in a 96-well plate (#353296; Falcon) one day before infection. Cells were infected with *L. pneumophila* strains expressing luciferase at a MOI of 0.5, then incubated at 37°C under 5% CO_2. Intracellular bacterial growth was monitored by luminescence using a microplate reader (GloMax Explorer; Promega).

Quantification and statistical analysis

Welch's t tests were performed on all microscopy quantifications using Prism 9 software with data from three independent infection experiments. P values less than 0.05 were considered significant, with annotations as follows: * ($p < 0.05$), ** ($p < 0.01$), *** ($p < 0.001$, **** ($p < 0.0001$).

Supplementary Material

Refer to Web version on PubMed Central for supplementary material.

ACKNOWLEDGEMENTS

We thank R. Klevit, D. Komander, and T. Mund for sharing expression plasmids, K. Arasaki for sharing the HeLa-FcγRII cell line, and X.T. Bui for assistance with BMDM preparation. We thank members of our laboratories and the Seattle Ub Research Group for helpful discussions. Use of the Stanford Synchrotron Radiation Lightsource, SLAC National Accelerator Laboratory, is supported by the U.S. DOE under Contract No. DE-AC02-76SF00515. The SSRL Structural Molecular Biology Program is supported by the DOE and the NIH (P30GM133894). This work was supported by the Takeda Science Foundation (TKu), MEXT/JSPS KAKENHI grants (19H03469 to TKu), Oregon Health & Science University (JNP), The Collins Medical Trust (JNP), and NIGMS (R35GM142486 to JNP).

REFERENCES

1. Popovic D, Vucic D, and Dikic I (2014). Ubiquitination in disease pathogenesis and treatment. Nat. Med 20, 1242–1253. 10.1038/nm.3739. [PubMed: 25375928]
2. Clague MJ, Heride C, and Urbé S (2015). The demographics of the ubiquitin system. Trends Cell Biol 25, 417–426. 10.1016/j.tcb.2015.03.002. [PubMed: 25906909]
3. Komander D, and Rape M (2012). The Ubiquitin Code. Annu. Rev. Biochem 81, 203–229. 10.1146/annurev-biochem-060310-170328. [PubMed: 22524316]
4. Xu P, Duong DM, Seyfried NT, Cheng D, Xie Y, Robert J, Rush J, Hochstrasser M, Finley D, and Peng J (2009). Quantitative proteomics reveals the function of unconventional ubiquitin chains in proteasomal degradation. Cell 137, 133–145. 10.1016/j.cell.2009.01.041. [PubMed: 19345192]
5. Wagner SA, Beli P, Weinert BT, Nielsen ML, Cox J, Mann M, and Choudhary C (2011). A proteome-wide, quantitative survey of in vivo ubiquitylation sites reveals widespread regulatory roles. Mol. Cell Proteomics 10, M111.013284. 10.1074/mcp.M111.013284.
6. Roscoe BP, Thayer KM, Zeldovich KB, Fushman D, and Bolon DNA (2013). Analyses of the effects of all ubiquitin point mutants on yeast growth rate. J. Mol. Biol 425, 1363–1377. 10.1016/j.jmb.2013.01.032. [PubMed: 23376099]
7. Meza Gutierrez F, Simsek D, Mizrak A, Deutschbauer A, Braberg H, Johnson J, Xu J, Shales M, Nguyen M, Tamse-Kuehn R, et al. (2018). Genetic analysis reveals functions of atypical polyubiquitin chains. Elife 7, 875. 10.7554/eLife.42955.
8. Swatek KN, and Komander D (2016). Ubiquitin modifications. Cell Research 26, 399–422. 10.1038/cr.2016.39. [PubMed: 27012465]
9. Kim W, Bennett EJ, Huttlin EL, Guo A, Li J, Possemato A, Sowa ME, Rad R, Rush J, Comb MJ, et al. (2011). Systematic and quantitative assessment of the ubiquitin-modified proteome. Mol. Cell 44, 325–340. 10.1016/j.molcel.2011.08.025. [PubMed: 21906983]
10. Ordureau A, Sarraf SA, Duda DM, Heo J-M, Jedrychowski MP, Sviderskiy VO, Olszewski JL, Koerber JT, Xie T, Beausoleil SA, et al. (2014). Quantitative proteomics reveal a feedforward mechanism for mitochondrial PARKIN translocation and ubiquitin chain synthesis. Mol. Cell 56, 360–375. 10.1016/j.molcel.2014.09.007. [PubMed: 25284222]
11. Elia AEH, Boardman AP, Wang DC, Huttlin EL, Everley RA, Dephoure N, Zhou C, Koren I, Gygi SP, and Elledge SJ (2015). Quantitative Proteomic Atlas of Ubiquitination and Acetylation in the DNA Damage Response. Mol. Cell 59, 867–881. 10.1016/j.molcel.2015.05.006. [PubMed: 26051181]

12. Heidelberger JB, Voigt A, Borisova ME, Petrosino G, Ruf S, Wagner SA, and Beli P (2018). Proteomic profiling of VCP substrates links VCP to K6-linked ubiquitylation and c-Myc function. EMBO Rep 19. 10.15252/embr.201744754.

13. Michel MA, Swatek KN, Hospenthal MK, and Komander D (2017). Ubiquitin Linkage-Specific Affimers Reveal Insights into K6-Linked Ubiquitin Signaling. Mol. Cell 68, 233–246.e235. 10.1016/j.molcel.2017.08.020. [PubMed: 28943312]

14. Bingol B, Tea JS, Phu L, Reichelt M, Bakalarski CE, Song Q, Foreman O, Kirkpatrick DS, and Sheng M (2014). The mitochondrial deubiquitinase USP30 opposes parkin-mediated mitophagy. Nature 510, 370–375. 10.1038/nature13418. [PubMed: 24896179]

15. Cunningham CN, Baughman JM, Phu L, Tea JS, Yu C, Coons M, Kirkpatrick DS, Bingol B, and Corn JE (2015). USP30 and parkin homeostatically regulate atypical ubiquitin chains on mitochondria. Nat. Cell Biol 17, 160–169. 10.1038/ncb3097. [PubMed: 25621951]

16. Gersch M, Gladkova C, Schubert AF, Michel MA, Maslen S, and Komander D (2017). Mechanism and regulation of the Lys6-selective deubiquitinase USP30. Nat. Struct. Mol. Biol 24, 920–930. 10.1038/nsmb.3475. [PubMed: 28945249]

17. Durcan TM, Tang MY, Pérusse JR, Dashti EA, Aguileta MA, McLelland G-L, Gros P, Shaler TA, Faubert D, Coulombe B, et al. (2014). USP8 regulates mitophagy by removing K6-linked ubiquitin conjugates from parkin. EMBO J 33, 2473–2491. 10.15252/embj.201489729. [PubMed: 25216678]

18. Wu-Baer F, Lagrazon K, Yuan W, and Baer R (2003). The BRCA1/BARD1 heterodimer assembles polyubiquitin chains through an unconventional linkage involving lysine residue K6 of ubiquitin 278, 34743–34746. 10.1074/jbc.C300249200.

19. Morris JR, and Solomon E (2004). BRCA1 : BARD1 induces the formation of conjugated ubiquitin structures, dependent on K6 of ubiquitin, in cells during DNA replication and repair. Hum. Mol. Genet 13, 807–817. 10.1093/hmg/ddh095. [PubMed: 14976165]

20. Nishikawa H, Ooka S, Sato K, Arima K, Okamoto J, Klevit RE, Fukuda M, and Ohta T (2004). Mass spectrometric and mutational analyses reveal Lys-6-linked polyubiquitin chains catalyzed by BRCA1-BARD1 ubiquitin ligase. J. Biol. Chem 279, 3916–3924. 10.1074/jbc.M308540200. [PubMed: 14638690]

21. Jäckl M, Stollmaier C, Strohäker T, Hyz K, Maspero E, Polo S, and Wiesner S (2018). β-Sheet Augmentation Is a Conserved Mechanism of Priming HECT E3 Ligases for Ubiquitin Ligation. J. Mol. Biol 430, 3218–3233. 10.1016/j.jmb.2018.06.044. [PubMed: 29964046]

22. Elliott PR (2016). Molecular basis for specificity of the Met1-linked polyubiquitin signal. Biochem. Soc. Trans 44, 1581–1602. 10.1042/BST20160227. [PubMed: 27913667]

23. Deol KK, Lorenz S, and Strieter ER (2019). Enzymatic Logic of Ubiquitin Chain Assembly. Front Physiol 10, 835. 10.3389/fphys.2019.00835. [PubMed: 31333493]

24. Mevissen TET, and Komander D (2017). Mechanisms of Deubiquitinase Specificity and Regulation. Annu. Rev. Biochem 86, 159–192. 10.1146/annurev-biochem-061516-044916. [PubMed: 28498721]

25. Franklin TG, and Pruneda JN (2021). Bacteria make surgical strikes on host ubiquitin signaling. PLoS Pathog 17, e1009341. 10.1371/journal.ppat.1009341. [PubMed: 33735219]

26. Lin DY-W, Diao J, Zhou D, and Chen J (2011). Biochemical and structural studies of a HECT-like ubiquitin ligase from Escherichia coli O157:H7. J. Biol. Chem 286, 441–449. 10.1074/jbc.M110.167643. [PubMed: 20980253]

27. Qiu J, and Luo Z-Q (2017). Hijacking of the Host Ubiquitin Network by Legionella pneumophila. Front Cell Infect Microbiol 7, 487. 10.3389/fcimb.2017.00487. [PubMed: 29376029]

28. Wan M, Wang X, Huang C, Xu D, Wang Z, Zhou Y, and Zhu Y (2019). A bacterial effector deubiquitinase specifically hydrolyses linear ubiquitin chains to inhibit host inflammatory signalling. Nat Microbiol 4, 1282–1293. 10.1038/s41564-019-0454-1. [PubMed: 31110362]

29. Kitao T, Nagai H, and Kubori T (2020). Divergence of Legionella Effectors Reversing Conventional and Unconventional Ubiquitination. Front Cell Infect Microbiol 10, 448. 10.3389/fcimb.2020.00448. [PubMed: 32974222]

30. Kubori T, Kitao T, Ando H, and Nagai H (2018). LotA, a Legionella deubiquitinase, has dual catalytic activity and contributes to intracellular growth. Cell. Microbiol 20, e12840. 10.1111/cmi.12840. [PubMed: 29543380]

31. Ma K, Zhen X, Zhou B, Gan N, Cao Y, Fan C, Ouyang S, Luo Z-Q, and Qiu J (2020). The bacterial deubiquitinase Ceg23 regulates the association of Lys-63-linked polyubiquitin molecules on the Legionella phagosome. J. Biol. Chem 295, 1646–1657. 10.1074/jbc.RA119.011758. [PubMed: 31907282]

32. Schubert AF, Nguyen JV, Franklin TG, Geurink PP, Roberts CG, Sanderson DJ, Miller LN, Ovaa H, Hofmann K, Pruneda JN, et al. (2020). Identification and characterization of diverse OTU deubiquitinases in bacteria. EMBO J 81, e105127. 10.15252/embj.2020105127.

33. Shin D, Bhattacharya A, Cheng Y-L, Alonso MC, Mehdipour AR, van der Heden van Noort GJ, Ovaa H, Hummer G, and Dikic I (2020). Bacterial OTU deubiquitinases regulate substrate ubiquitination upon Legionella infection. Elife 9. 10.7554/eLife.58277.

34. Liu S, Luo J, Zhen X, Qiu J, Ouyang S, and Luo Z-Q (2020). Interplay between bacterial deubiquitinase and ubiquitin E3 ligase regulates ubiquitin dynamics on Legionella phagosomes. Elife 9. 10.7554/eLife.58114.

35. Hermanns T, Woiwode I, Guerreiro RF, Vogt R, Lammers M, and Hofmann K (2020). An evolutionary approach to systematic discovery of novel deubiquitinases, applied to Legionella. Life Sci Alliance 3. 10.26508/lsa.202000838.

36. Ekkebus R, van Kasteren SI, Kulathu Y, Scholten A, Berlin I, Geurink PP, de Jong A, Goerdayal S, Neefjes J, Heck AJR, et al. (2013). On terminal alkynes that can react with active-site cysteine nucleophiles in proteases. J. Am. Chem. Soc 135, 2867–2870. 10.1021/ja309802n. [PubMed: 23387960]

37. Geurink PP, Oualid, El F, Jonker A, Hameed DS, and Ovaa H (2012). A general chemical ligation approach towards isopeptide-linked ubiquitin and ubiquitin-like assay reagents. Chembiochem 13, 293–297. 10.1002/cbic.201100706. [PubMed: 22213387]

38. Mevissen TET, Hospenthal MK, Geurink PP, Elliott PR, Akutsu M, Arnaudo N, Ekkebus R, Kulathu Y, Wauer T, Oualid, El F, et al. (2013). OTU deubiquitinases reveal mechanisms of linkage specificity and enable ubiquitin chain restriction analysis. Cell 154, 169–184. 10.1016/j.cell.2013.05.046. [PubMed: 23827681]

39. Békés M, Rut W, Kasperkiewicz P, Mulder MPC, Ovaa H, Drag M, Lima CD, and Huang TT (2015). SARS hCoV papain-like protease is a unique Lys48 linkage-specific di-distributive deubiquitinating enzyme. Biochem. J 468, 215–226. 10.1042/BJ20141170. [PubMed: 25764917]

40. Abdul Rehman SA, Kristariyanto YA, Choi S-Y, Nkosi PJ, Weidlich S, Labib K, Hofmann K, and Kulathu Y (2016). MINDY-1 Is a Member of an Evolutionarily Conserved and Structurally Distinct New Family of Deubiquitinating Enzymes. Mol. Cell 63, 146–155. 10.1016/j.molcel.2016.05.009. [PubMed: 27292798]

41. Virdee S, Ye Y, Nguyen DP, Komander D, and Chin JW (2010). Engineered diubiquitin synthesis reveals Lys29-isopeptide specificity of an OTU deubiquitinase. Nat. Chem. Biol 6, 750–757. 10.1038/nchembio.426. [PubMed: 20802491]

42. Keusekotten K, Elliott PR, Glockner L, Fiil BK, Damgaard RB, Kulathu Y, Wauer T, Hospenthal MK, Gyrd-Hansen M, Krappmann D, et al. (2013). OTULIN antagonizes LUBAC signaling by specifically hydrolyzing Met1-linked polyubiquitin. Cell 153, 1312–1326. 10.1016/j.cell.2013.05.014. [PubMed: 23746843]

43. Pruneda JN, Durkin CH, Geurink PP, Ovaa H, Santhanam B, Holden DW, and Komander D (2016). The Molecular Basis for Ubiquitin and Ubiquitin-like Specificities in Bacterial Effector Proteases. Mol. Cell 63, 261–276. 10.1016/j.molcel.2016.06.015. [PubMed: 27425412]

44. Mevissen TET, Kulathu Y, Mulder MPC, Geurink PP, maslen SL, Gersch M, Elliott PR, burke JE, van Tol BDM, Akutsu M, et al. (2016). Molecular basis of Lys11-polyubiquitin specificity in the deubiquitinase Cezanne. Nature 538, 402–405. 10.1038/nature19836. [PubMed: 27732584]

45. Hospenthal MK, Freund SMV, and Komander D (2013). Assembly, analysis and architecture of atypical ubiquitin chains. Nat. Struct. Mol. Biol 20, 555–565. 10.1038/nsmb.2547. [PubMed: 23563141]

46. Hospenthal MK, Mevissen TET, and Komander D (2015). Deubiquitinase-based analysis of ubiquitin chain architecture using Ubiquitin Chain Restriction (UbiCRest). Nat Protoc 10, 349–361. 10.1038/nprot.2015.018. [PubMed: 25633630]
47. Michel MA, Elliott PR, Swatek KN, Simicek M, Pruneda JN, Wagstaff JL, Freund SMV, and Komander D (2015). Assembly and specific recognition of k29- and k33-linked polyubiquitin. Mol. Cell 58, 95–109. 10.1016/j.molcel.2015.01.042. [PubMed: 25752577]
48. Akutsu M, Ye Y, Virdee S, Chin JW, and Komander D (2011). Molecular basis for ubiquitin and ISG15 cross-reactivity in viral ovarian tumor domains. Proc. Natl. Acad. Sci. U.S.A 108, 2228–2233. 10.1073/pnas.1015287108. [PubMed: 21266548]
49. Grabarczyk DB, Petrova OA, Deszcz L, Kurzbauer R, Murphy P, Ahel J, Vogel A, Gogova R, Faas V, Kordic D, et al. (2021). HUWE1 employs a giant substrate-binding ring to feed and regulate its HECT E3 domain. Nat. Chem. Biol 17, 1084–1092. 10.1038/s41589-021-00831-5. [PubMed: 34294896]
50. Takekawa N, Kubori T, Iwai T, Nagai H, and Imada K (2022). Structural Basis of Ubiquitin Recognition by a Bacterial Ovarian Tumor Deubiquitinase LotA. J. Bacteriol 204, e0037621. 10.1128/JB.00376-21. [PubMed: 34633867]
51. Juang Y-C, Landry M-C, Sanches M, Vittal V, Leung CCY, Ceccarelli DF, Mateo A-RF, Pruneda JN, Mao DYL, Szilard RK, et al. (2012). OTUB1 co-opts Lys48-linked ubiquitin recognition to suppress E2 enzyme function. Mol. Cell 45, 384–397. 10.1016/j.molcel.2012.01.011. [PubMed: 22325355]
52. Holm L (2020). Using Dali for Protein Structure Comparison. Methods Mol. Biol 2112, 29–42. 10.1007/978-1-0716-0270-6_3. [PubMed: 32006276]
53. Li Y, Okatsu K, Fukai S, and Sato Y (2021). Structural basis for specific recognition of K6-linked polyubiquitin chains by the TAB2 NZF domain. Biophys J 120, 3355–3362. 10.1016/j.bpj.2021.06.037. [PubMed: 34242591]
54. Berk JM, Lim C, Ronau JA, Chaudhuri A, Chen H, Beckmann JF, Loria JP, Xiong Y, and Hochstrasser M (2020). A deubiquitylase with an unusually high-affinity ubiquitin-binding domain from the scrub typhus pathogen Orientia tsutsugamushi. Nat Commun 11, 2343–17. 10.1038/s41467-020-15985-4. [PubMed: 32393759]
55. Dorer MS, Kirton D, Bader JS, and Isberg RR (2006). RNA interference analysis of Legionella in Drosophila cells: exploitation of early secretory apparatus dynamics. PLoS Pathog 2, e34. 10.1371/journal.ppat.0020034. [PubMed: 16652170]
56. Sato Y, Okatsu K, Saeki Y, Yamano K, Matsuda N, Kaiho A, Yamagata A, Goto-Ito S, Ishikawa M, Hashimoto Y, et al. (2017). Structural basis for specific cleavage of Lys6-linked polyubiquitin chains by USP30. Nat. Struct. Mol. Biol 24, 911–919. 10.1038/nsmb.3469. [PubMed: 28945247]
57. Manzanillo PS, Ayres JS, Watson RO, Collins AC, Souza G, Rae CS, Schneider DS, Nakamura K, Shiloh MU, and Cox JS (2013). The ubiquitin ligase parkin mediates resistance to intracellular pathogens. Nature 501, 512–516. 10.1038/nature12566. [PubMed: 24005326]
58. Thomas DR, Newton P, Lau N, and Newton HJ (2020). Interfering with Autophagy: The Opposing Strategies Deployed by Legionella pneumophila and Coxiella burnetii Effector Proteins. Front Cell Infect Microbiol 10, 599762. 10.3389/fcimb.2020.599762. [PubMed: 33251162]
59. Arasaki K, Mikami Y, Shames SR, Inoue H, Wakana Y, and Tagaya M (2017). Legionella effector Lpg1137 shuts down ER-mitochondria communication through cleavage of syntaxin 17. Nat Commun 8, 15406–15412. 10.1038/ncomms15406. [PubMed: 28504273]
60. Celada A, Gray PW, Rinderknecht E, and Schreiber RD (1984). Evidence for a gamma-interferon receptor that regulates macrophage tumoricidal activity. J Exp Med 160, 55–74. 10.1084/jem.160.1.55. [PubMed: 6330272]
61. Kabsch W (2010). XDS. Acta Crystallogr. D Biol. Crystallogr 66, 125–132. 10.1107/S0907444909047337. [PubMed: 20124692]
62. Potterton L, Agirre J, Ballard C, Cowtan K, Dodson E, Evans PR, Jenkins HT, Keegan R, Krissinel E, Stevenson K, et al. (2018). CCP4i2: the new graphical user interface to the CCP4 program suite. Acta Crystallogr D Struct Biol 74, 68–84. 10.1107/S2059798317016035. [PubMed: 29533233]

63. Evans PR, and Murshudov GN (2013). How good are my data and what is the resolution? Acta Crystallogr. D Biol. Crystallogr 69, 1204–1214. 10.1107/S0907444913000061. [PubMed: 23793146]
64. Sheldrick GM (2010). Experimental phasing with SHELXC/D/E: combining chain tracing with density modification. Acta Crystallogr. D Biol. Crystallogr 66, 479–485. 10.1107/S0907444909038360. [PubMed: 20383001]
65. Langer G, Cohen SX, Lamzin VS, and Perrakis A (2008). Automated macromolecular model building for X-ray crystallography using ARP/wARP version 7. Nat Protoc 3, 1171–1179. 10.1038/nprot.2008.91. [PubMed: 18600222]
66. McCoy AJ, Grosse-Kunstleve RW, Adams PD, Winn MD, Storoni LC, and Read RJ (2007). Phaser crystallographic software. J Appl Crystallogr 40, 658–674. 10.1107/S0021889807021206. [PubMed: 19461840]
67. Adams PD, Afonine PV, Bunkóczi G, Chen VB, Davis IW, Echols N, Headd JJ, Hung L-W, Kapral GJ, Grosse-Kunstleve RW, et al. (2010). PHENIX: a comprehensive Python-based system for macromolecular structure solution. Acta Crystallogr. D Biol. Crystallogr 66, 213–221. 10.1107/S0907444909052925. [PubMed: 20124702]
68. Emsley P, Lohkamp B, Scott WG, and Cowtan K (2010). Features and development of Coot. Acta Crystallogr. D Biol. Crystallogr 66, 486–501. 10.1107/S0907444910007493. [PubMed: 20383002]
69. Berger KH, and Isberg RR (1993). Two distinct defects in intracellular growth complemented by a single genetic locus in Legionella pneumophila. Mol. Microbiol 7, 7–19. 10.1111/j.1365-2958.1993.tb01092.x. [PubMed: 8382332]
70. Zuckman DM, Hung JB, and Roy CR (1999). Pore-forming activity is not sufficient for Legionella pneumophila phagosome trafficking and intracellular growth. Mol. Microbiol 32, 990–1001. 10.1046/j.1365-2958.1999.01410.x. [PubMed: 10361301]
71. Coers J, Vance RE, Fontana MF, and Dietrich WF (2007). Restriction of Legionella pneumophila growth in macrophages requires the concerted action of cytokine and Naip5/Ipaf signalling pathways. Cell. Microbiol 9, 2344–2357. 10.1111/j.1462-5822.2007.00963.x. [PubMed: 17506816]
72. Horwitz MA (1983). The Legionnaires' disease bacterium (Legionella pneumophila) inhibits phagosome-lysosome fusion in human monocytes. J Exp Med 158, 2108–2126. 10.1084/jem.158.6.2108. [PubMed: 6644240]
73. Kelley LA, Mezulis S, Yates CM, Wass MN, and Sternberg MJE (2015). The Phyre2 web portal for protein modeling, prediction and analysis. Nat Protoc 10, 845–858. 10.1038/nprot.2015.053. [PubMed: 25950237]
74. Studier FW (2005). Protein production by auto-induction in high density shaking cultures. Protein Expr Purif 41, 207–234. 10.1016/j.pep.2005.01.016. [PubMed: 15915565]
75. Wilkinson KD, Gan-Erdene T, and Kolli N (2005). Derivitization of the C-terminus of ubiquitin and ubiquitin-like proteins using intein chemistry: methods and uses. Meth. Enzymol 399, 37–51. 10.1016/S0076-6879(05)99003-4.
76. Michel MA, Komander D, and Elliott PR (2018). Enzymatic Assembly of Ubiquitin Chains. Methods Mol. Biol 1844, 73–84. 10.1007/978-1-4939-8706-1_6. [PubMed: 30242704]
77. Pruneda JN, and Komander D (2019). Evaluating enzyme activities and structures of DUBs. Meth. Enzymol 618, 321–341. 10.1016/bs.mie.2019.01.001.
78. Basters A, Geurink PP, Oualid, El F, Ketscher L, Casutt MS, Krause E, Ovaa H, Knobeloch K-P, and Fritz G (2014). Molecular characterization of ubiquitin-specific protease 18 reveals substrate specificity for interferon-stimulated gene 15. FEBS J 281, 1918–1928. 10.1111/febs.12754. [PubMed: 24533902]
79. Vijay-Kumar S, Bugg CE, and Cook WJ (1987). Structure of ubiquitin refined at 1.8 A resolution. J. Mol. Biol 194, 531–544. 10.1016/0022-2836(87)90679-6. [PubMed: 3041007]
80. Merriam JJ, Mathur R, Maxfield-Boumil R, and Isberg RR (1997). Analysis of the Legionella pneumophila fliI gene: intracellular growth of a defined mutant defective for flagellum biosynthesis. Infect. Immun 65, 2497–2501. 10.1128/iai.65.6.2497-2501.1997. [PubMed: 9169800]

Highlights:

- *L. pneumophila* LotA encodes two functionally-distinct deubiquitinases
- LotA's specificity for K6-linked poly-ubiquitin makes it a valuable research tool
- Structures reveal that K6 specificity arises from substrate-assisted catalysis
- LotA restricts K6 poly-ubiquitin and VCP recruitment during infection

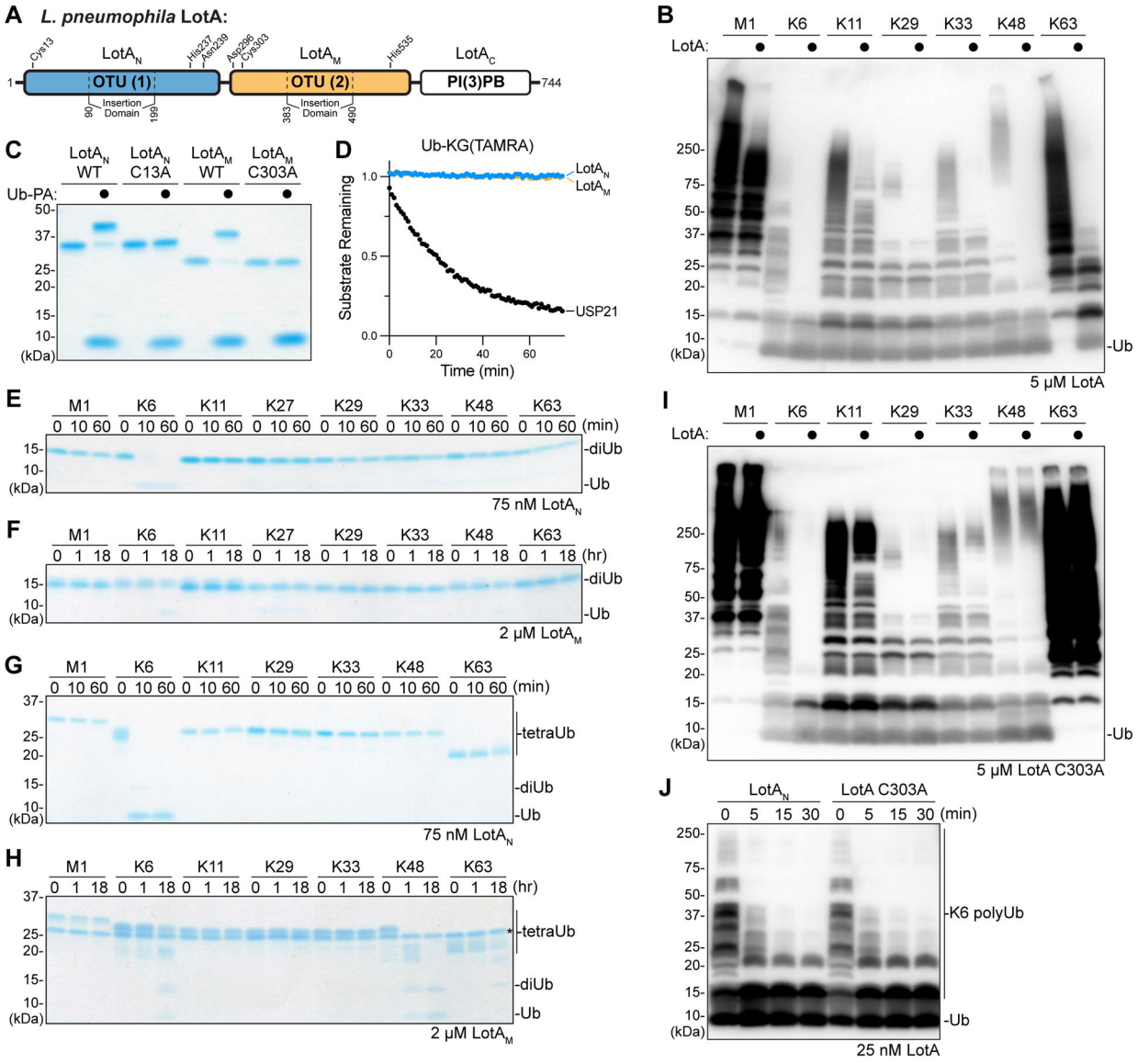

Figure 1: Separation of LotA deubiquitinase activities

A. Domain architecture of *L. pneumophila* LotA, with catalytic triad residues annotated for each OTU domain.

B. Homogeneous assemblies of seven polyUb linkage types were treated with a high concentration (5 μM) of full length LotA for 2 h before the reactions were quenched and visualized by anti-Ub Western blot.

C. Coomassie-stained SDS-PAGE gel showing purified constructs of $LotA_N$ (1–300) and $LotA_M$ (287–543), alongside their catalytically-inactive variants. Reactivity with the Ub-PA activity-based probe is assessed by a shift in mobility.

D. Ub-KG(TAMRA) cleavage assay monitored by fluorescence polarization. Activity was measured using 1 μM $LotA_N$, 1 μM $LotA_M$, or 100 nM USP21 as a control DUB.

E-F. Gel-based specificity analysis against all eight canonical diUb linkages. Reactions containing the indicated concentrations of $LotA_N$ (**D**) and $LotA_M$ (**E**) were sampled at the indicated timepoints, quenched, and resolved by SDS-PAGE with Coomassie staining.

G-H. Gel-based specificity analysis against seven tetraUb linkages. Reactions containing the indicated concentrations of $LotA_N$ (**F**) and $LotA_M$ (**G**) were sampled at the indicated timepoints, quenched, and resolved by SDS-PAGE with Coomassie staining. Note that some tetraUb chains migrate differently based on the linkage site, as observed previously[38,45,46].

I. Homogeneous assemblies of seven polyUb linkage types were treated with a high concentration (5 μM) of full length LotA C303A for 2 h before the reactions were quenched and visualized by anti-Ub Western blot.

J. A homogeneous assembly of K6-linked polyUb was treated with either $LotA_N$ or the full length LotA C303A variant at 25 nM. Reaction samples were collected and visualized by anti-Ub Western blot.

See also Figure S1.

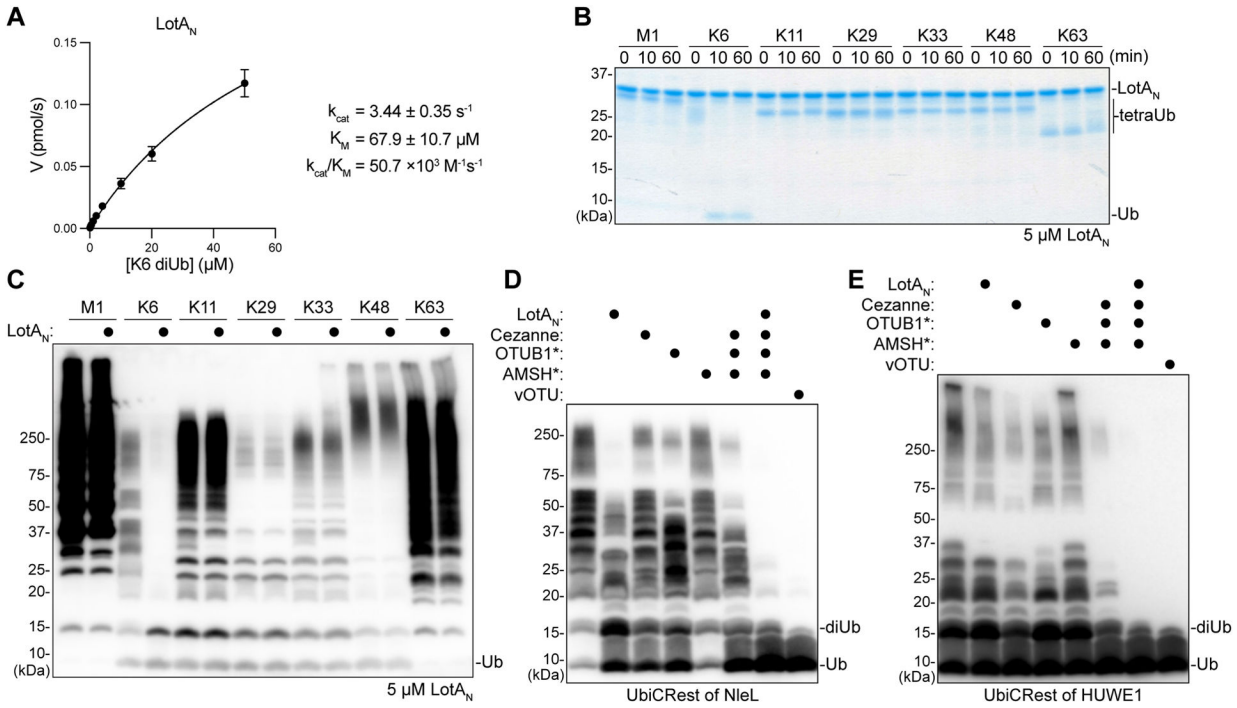

Figure 2: Application of LotA$_N$ K6 specificity for UbiCRest analysis

A. Kinetic parameters of LotA$_N$ (1–300) measured by changes in fluorescence polarization of labeled K6 diUb. Initial rates of diUb cleavage were measured over a range of substrate concentrations and fit to a Michaelis-Menten model. Error bars represent standard deviation over three measurements, each made in triplicate.

B. Gel-based specificity analysis against seven tetraUb linkages. Reactions containing a high concentration (5 μM) of LotA$_N$ were sampled at the indicated timepoints, quenched, and resolved by SDS-PAGE with Coomassie staining.

C. Homogeneous assemblies of seven polyUb linkage types were treated with a high concentration (5 μM) of LotA$_N$ for 2 h before the reactions were quenched and visualized by anti-Ub Western blot.

D. UbiCRest analysis of an NleL ligase assembly with 1 μM K6-specific LotA$_N$, K11-specific Cezanne, K48-specific OTUB1*, K63-specific AMSH*, nonspecific vOTU, or the indicated combinations. Reactions were visualized by anti-Ub Western blot. Cleavage of NleL-assembled polyUb can be observed by a decrease in the “smear” or by a reappearance of monoUb.

E. UbiCRest analysis of a HUWE1 ligase assembly with 1 μM K6-specific LotA$_N$, K11-specific Cezanne, K48-specific OTUB1*, K63-specific AMSH*, nonspecific vOTU, or the indicated combinations. Reactions were visualized by anti-Ub Western blot. Cleavage of HUWE1-assembled polyUb can be observed by a decrease in the “smear” or by a reappearance of monoUb.

See also Figure S2.

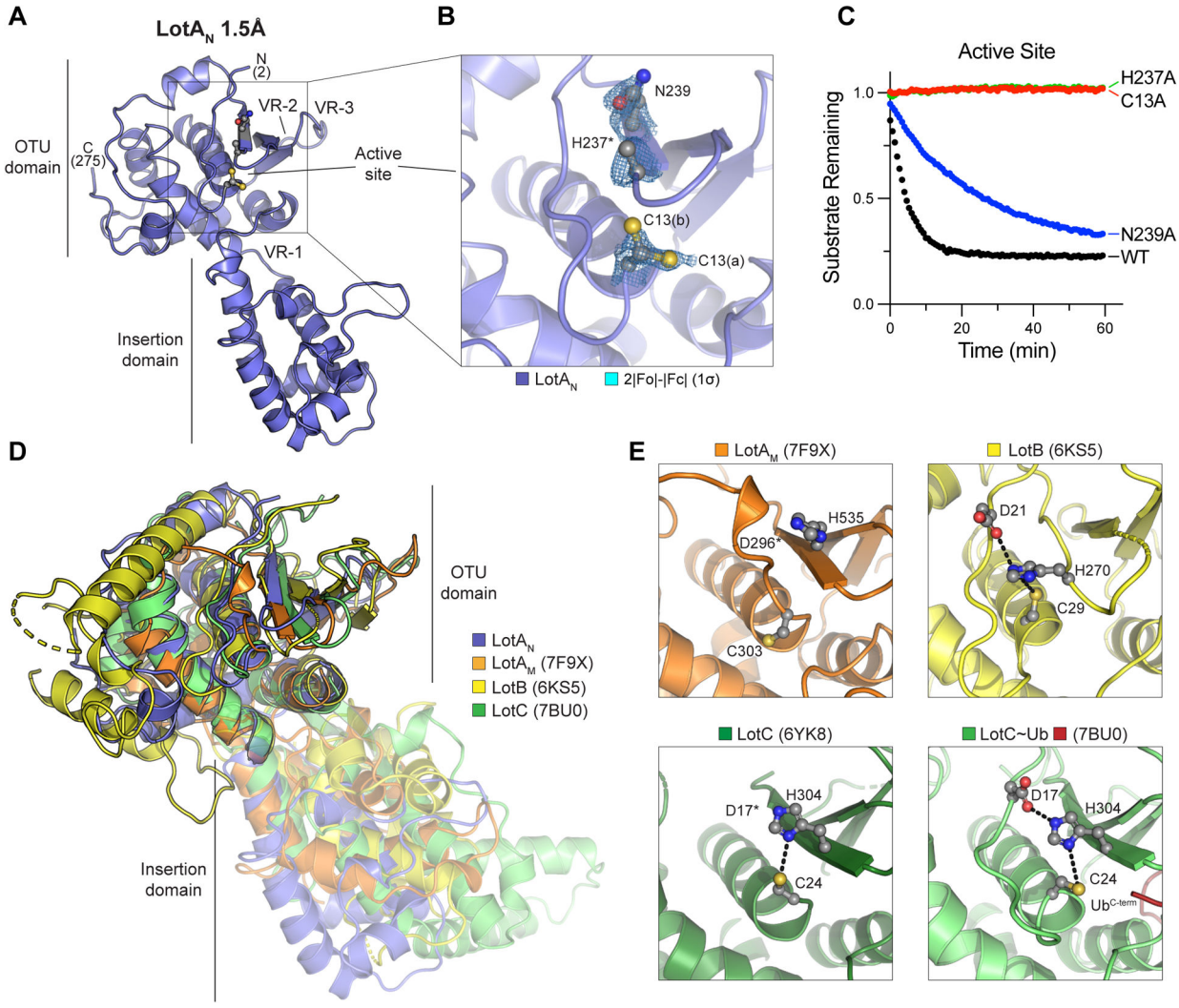

Figure 3: Crystal structure of the LotA$_N$ OTU domain

A. 1.5Å crystal structure of LotA (1–294) labeled with visible termini, domain architecture, active site, and OTU variable regions (VR1–3) described previously[32].

B. Close-up view of the LotA$_N$ active site with 2|Fo|-|Fc| electron density overlaid at 1σ for catalytic triad residues. Alternate conformations of the C13 side chain (a and b) are observed, whereas density for the H237 imidazole ring is absent.

C. Cleavage of fluorescent K6 diUb by the indicated LotA$_N$ active site variants at 10 nM concentration monitored by fluorescence polarization.

D. Structural overlay of LotA$_N$ (blue), LotA$_M$ (PDB 7F9X, orange), LotB (PDB 6KS5, yellow), and LotC (PDB 7BU0, green). Structures were aligned by their core OTU domains to demonstrate variability in the insertion domains.

E. Close-up views of the LotA$_M$, LotB, LotC (PDB 6YK8), and Ub-bound LotC (PDB 7BU0) active sites. Catalytic triad residues are shown in ball-and-stick representation, with hydrogen bonds indicated by dashed lines.

See also Figure S3.

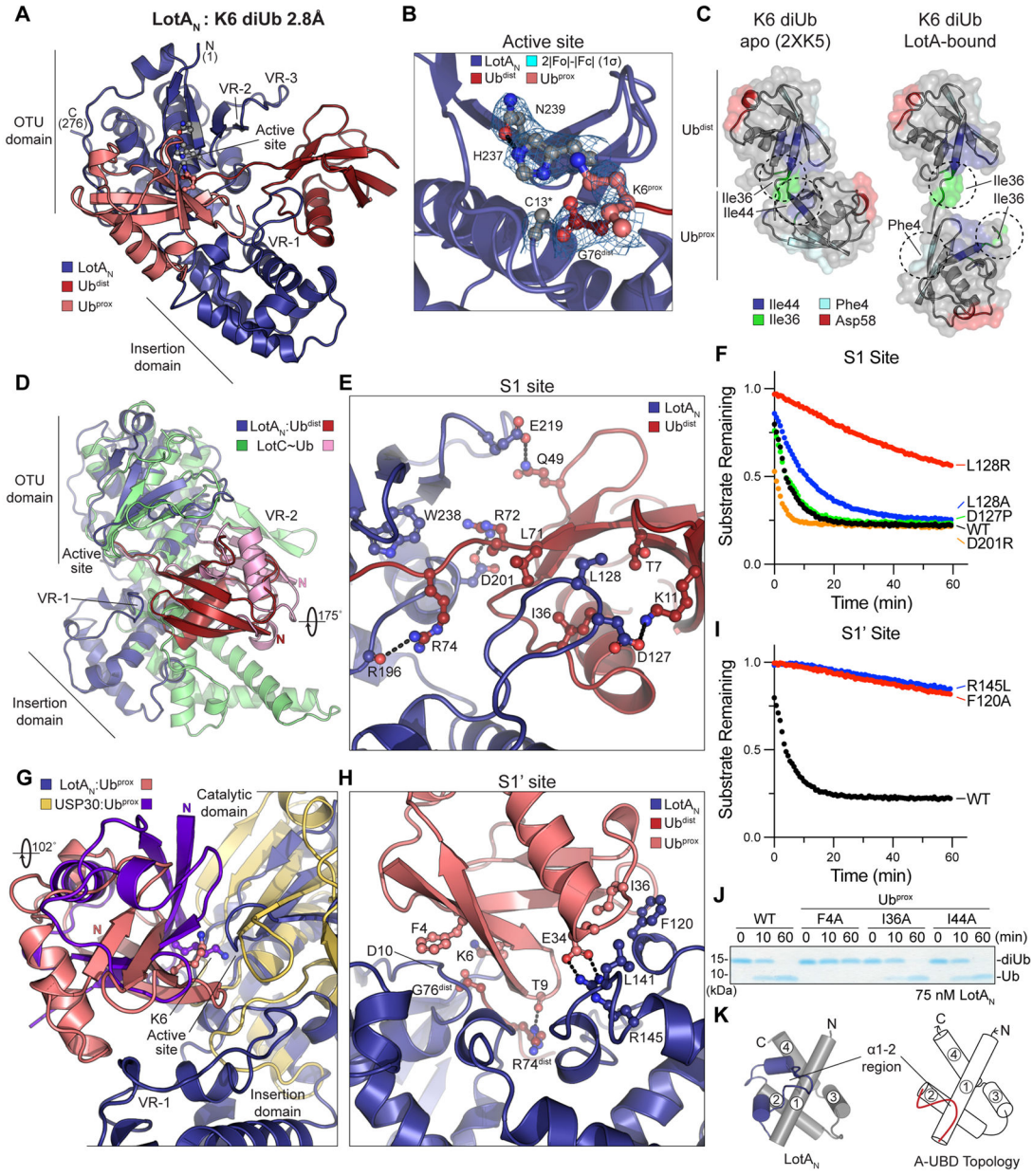

Figure 4: Crystal structure of the LotA$_N$ OTU domain bound to K6 diUb

A. 2.8Å crystal structure of LotA$_N$ (1–276, blue) bound to K6 diUb (shades of red). The structure is labeled with visible termini, domain architecture, active site, and OTU variable regions (VR1–3).

B. Close-up view of the K6 diUb-bound LotA$_N$ active site with 2|Fo|-|Fc| electron density overlaid at 1σ for catalytic triad residues. The K6 side chain of Ub^{prox} and C-terminus of Ub^{dist} are also shown with overlaid electron density. The LotA$_N$ catalytically inactive C13A variant was used to preserve the diUb linkage.

C. Crystal structures of K6 diUb in isolation (PDB 2XK5) and bound to LotA$_N$, aligned by their Ub^{dist} moieties (top). Availability and orientation of common interaction surfaces are

shown, with dashed circles indicating the surfaces utilized by either Ub:Ub or $LotA_N$:Ub interaction.

D. Structural overlay of $LotA_N$ (blue) and LotC (green) bound to their respective distal Ub moieties (red and pink, respectively). The structures are aligned on their core OTU domains, and highlight large differences in Ub orientation, insertion domains, and use of variable regions.

E. Close-up view of the $LotA_N$ S1 site (blue) bound to Ub^{dist} (red). Interacting residues are shown in ball-and-stick representation, with hydrogen bonds indicated by dashed lines.

F. Cleavage of fluorescent K6 diUb by the indicated $LotA_N$ S1 site variants at 10 nM concentration monitored by fluorescence polarization.

G. Structural overlay of $LotA_N$ (blue) and human USP30 (tan) bound to their respective distal Ub moieties (salmon and purple, respectively). The structures are aligned on their core catalytic domains, and highlight large differences in Ub orientation and features of their S1' sites.

H. Close-up view of the $LotA_N$ S1' site (blue) bound to Ub^{prox} (salmon). Interacting residues are shown in ball-and-stick representation, with hydrogen bonds indicated by dashed lines.

I. Cleavage of fluorescent K6 diUb by the indicated $LotA_N$ S1' site variants at 10 nM concentration monitored by fluorescence polarization. These data were collected in parallel with those presented in (**F**), and the WT dataset is shown again for reference.

J. Gel-based $LotA_N$ cleavage assay of K6 diUb variants with indicated Ub^{prox} mutations. Reactions were quenched at the indicated times and visualized by SDS PAGE with Coomassie staining.

K. Underlying helical domain architecture of the $LotA_N$ (left) and stereotypical (right) adaptive Ub-binding domain (A-UBD), with helices labeled and the Ub-binding α1–2 regions shown in color.

See also Figure S4.

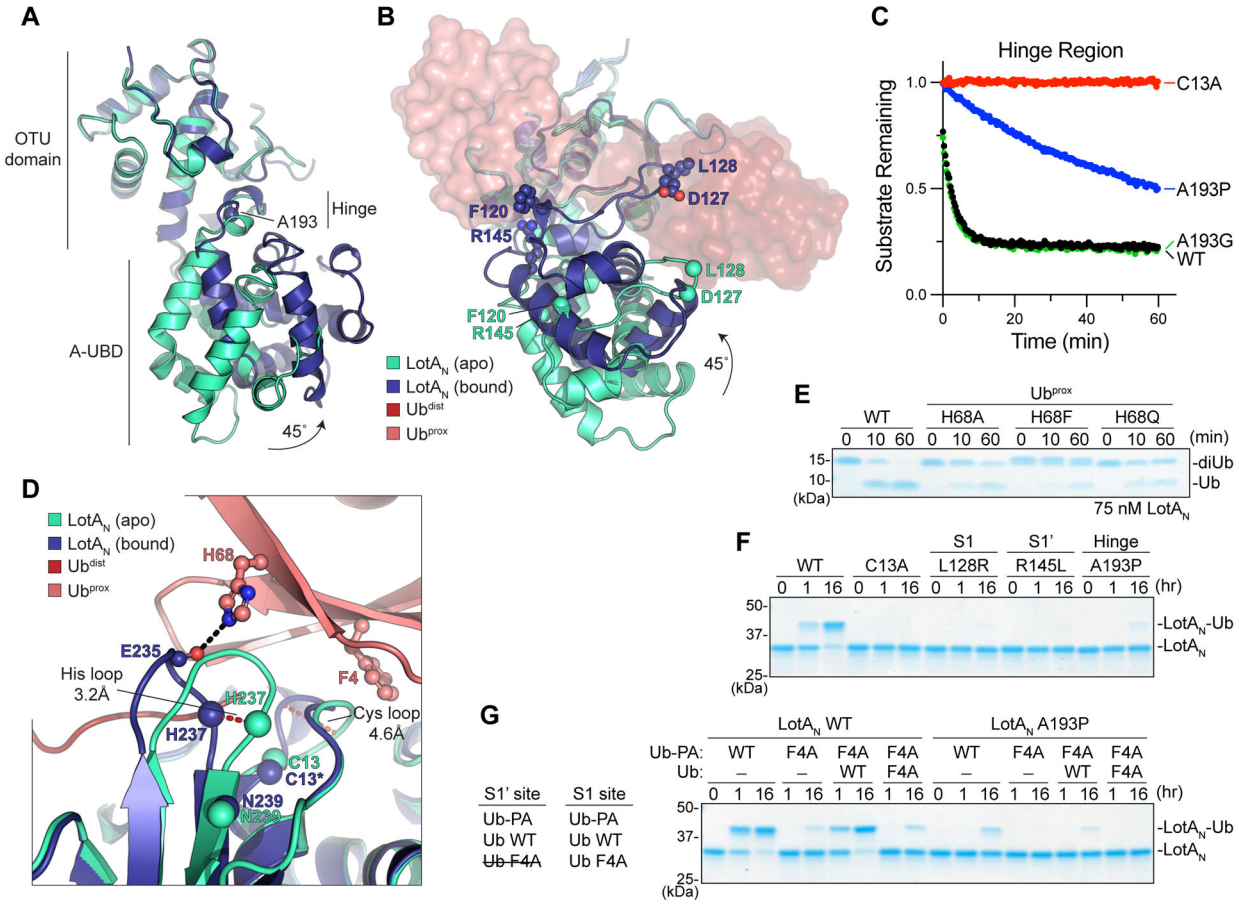

Figure 5: Conformational changes of LotA$_N$ during catalysis

A. Structural overlay of apo (cyan) and K6 diUb-bound (blue) LotA$_N$, aligned on their core OTU domains. A site for structure-guided mutation within the hinge region is shown.

B. As in (**A**), following ~90-degree rotation to visualize formation of the LotA$_N$ S1 and S1' Ub-binding sites upon rotation of the A-UBD.

C. Cleavage of fluorescent K6 diUb by the indicated LotA$_N$ hinge variants at 10 nM concentration monitored by fluorescence polarization.

D. Structural overlay of the active sites from apo (cyan) and K6 diUb-bound (blue) LotA$_N$, aligned on their core OTU domains. Conformational changes of the Cys and His loops that occur upon Ub binding (shades of red) are shown by red dashed lines. Distances of the Cys and His loop movements are measured by the Cα positions of LotA$_N$ H237 and G11, respectively. The Cα of LotA$_N$ catalytic triad residues are shown as spheres. Ub^{prox} residues opposing the rearranged LotA$_N$ loops are shown in ball-and-stick representation, with hydrogen bonds indicated as black dashed lines.

E. Gel-based LotA$_N$ cleavage assay of K6 diUb variants with indicated Ub^{prox} mutations. Reactions were quenched at the indicated times and visualized by SDS PAGE with Coomassie staining.

F. Ub-PA reactivity of LotA$_N$ wild-type alongside the indicated catalytic, S1 site, S1' site, and hinge mutations. Reactions were quenched at the indicated times and visualized by SDS PAGE with Coomassie staining.

G. Ub-PA reactivity assay combining the indicated $LotA_N$, Ub-PA, and Ub variants. *Left*, the ability of each Ub variant to competently bind the $LotA_N$ S1 or S1' site is listed.
See also Figure S5.

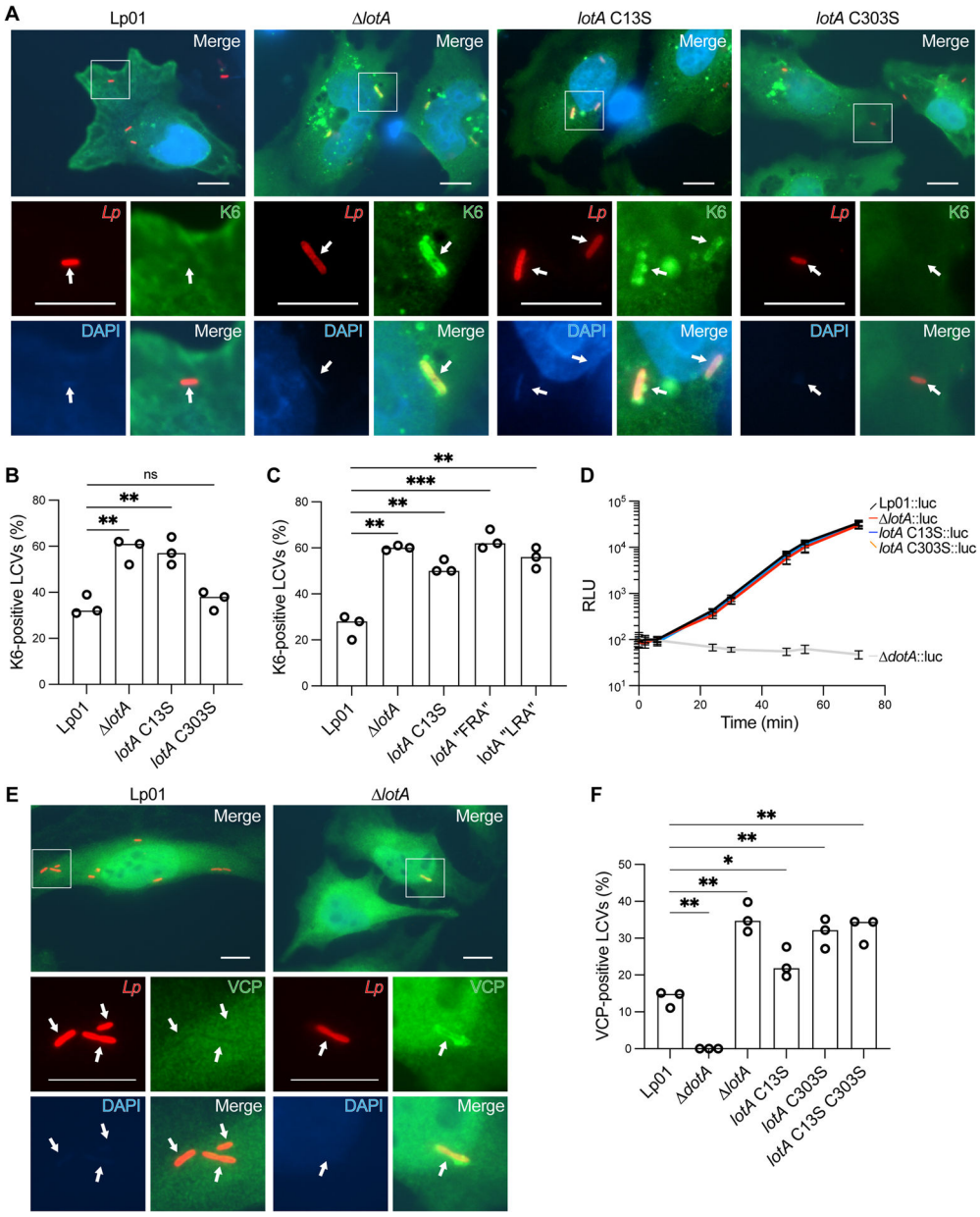

Figure 6: LotA$_N$ restriction of K6 polyUb during *L. pneumophila* infection

A. Representative images of HeLa FcγRII cells infected with the indicated *L. pneumophila* strains at an MOI of 2 for 4 h. Fixed cells were stained for *L. pneumophila* (red), HA-Ub-K6 (green), and DNA (blue). Arrows indicate the position of a bacterium in each channel. Images were collected at 100x magnification. Scale bars correspond to 10 μm.

B. Quantitation of K6-positive bacteria shown in (**A**). Infections were performed in triplicate and each value represents scoring from 100 LCVs. Significance was determined using a Welch's t-test.

C. Quantitation of K6-positive bacteria from HeLa FcγRII cells infected with the indicated *L. pneumophila* strains at an MOI of 2 for 4 h. Infections were performed in triplicate and

each value represents scoring from 100 LCVs. Significance was determined using a Welch's t-test.

D. Luciferase-expressing *L. pneumophila* strains were used to infect mouse BMDMs at an MOI of 0.5. Intracellular growth was monitored via bioluminescence changes over time. The mean relative luminescence unit (RLU) and standard deviation of eight independent experiments are shown.

E. Representative images of HeLa FcγRII cells infected with the indicated *L. pneumophila* strains at an MOI of 2 for 4 h. Fixed cells were stained for *L. pneumophila* (red), VCP (green), and DNA (blue). Arrows indicate the position of a bacterium in each channel. Images were collected at 100x magnification. Scale bars correspond to 10 μm.

F. Quantitation of VCP-positive bacteria shown in (**E**), alongside infections with a secretion-deficient Δ*dotA* strain and strains carrying mutations in the LotA active sites. Infections were performed in triplicate and each value represents scoring from 100 LCVs. Significance was determined using a Welch's t-test.

See also Figure S6.

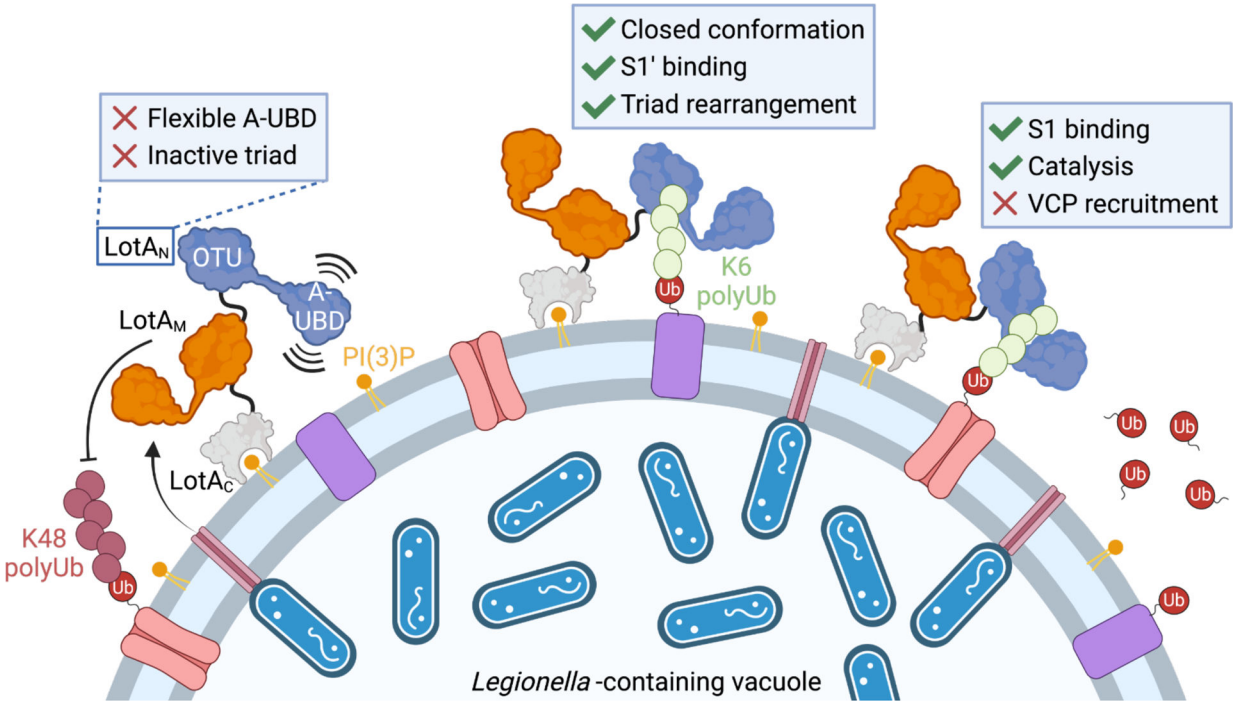

Figure 7: Model for LotA deubiquitinase activity

Secreted LotA localizes back to the cytosolic face of the LCV via the PI(3)P-binding LotA$_C$ domain. At the LCV, DUB activity of LotA$_M$ restricts long K48 and K63 polyUb. LotA$_N$ is kept inactive by a flexible A-UBD and inactive arrangement of the catalytic triad. Occupying a closed OTU:A-UBD conformation allows formation of an S1' Ub-binding site. Binding of a K6-linked Ub into the S1' site orients the LotA$_N$ catalytic triad, allowing for hydrolysis of K6 polyUb and prevention of VCP recruitment. Created with BioRender.com.

Table 1:

Data collection and refinement statistics

	$LotA_N$ (1–294)	**$LotA_N$ (1–276) : K6 diUb**
Data collection		
Wavelength	0.979460	0.979460
Space group	$P4_1\,2_1\,2$	$P4\,2\,2$
Cell dimensions		
a, *b*, *c* (Å)	86.25, 86.25, 92.30	127.28, 127.28, 77.99
α, β, γ (°)	90, 90, 90	90, 90, 90
Resolution (Å)	39.07–1.50 (1.50–1.53)	38.99–2.80 (2.80–2.95)
R_{merge}	0.035 (0.819)	0.257 (1.15)
$I/\sigma I$	26.6 (2.2)	6.4 (2.0)
Completeness (%)	99.9 (99.7)	99.9 (100)
Redundancy	6.5 (6.5)	6.5 (6.7)
Phasing		
Method	SAD	MR
SAD Resolution	1.50	-
SAD Anom completeness	99.6 (99.5)	-
SAD Anom multiplicity	3.4 (3.3)	-
SAD FOM	0.733	-
MR Search Models	-	$LotA_N$, Ub (1UBQ)
Refinement		
Resolution (Å)	35.59–1.50	38.99–2.80
No. unique reflections / test set	56168 / 2895	16316 / 822
R_{work}/R_{free}	0.195/0.221	0.207/0.259
No. atoms		
Protein	2174	3399
Ligand/ion	19	0
Water	286	59
B-factors		
Protein	32.81	47.04
Ligand/ion	54.93	-
Water	39.12	33.63
R.m.s. deviations		
Bond lengths (Å)	0.006	0.006
Bond angles (°)	0.77	1.04
Ramachandran statistics		
Favored / allowed / outliers	96.7 / 3.3 / 0	97.2 / 2.8 / 0

Values in parentheses are for highest resolution shell.

Key Resources Table

REAGENT or RESOURCE	SOURCE	IDENTIFIER
Antibodies		
Anti-Ubiquitin (clone Ubi-1)	MilliporeSigma	Cat#MAB1510-I
Anti-Mouse IgG, HRP conjugate	MilliporeSigma	Cat#12–349
Anti-Legionella	Scrum	Cat#17457
Anti-Legionella	BioAcademia	Cat#64–100
Anti-HA	MBL	Cat#561
Anti-VCP	Abcam	Cat#ab11433
Anti-Rabbit IgG, Alexa488 conjugate	Invitrogen	Cat#A11034
Anti-Rat IgG, Alexa 568 conjugate	Invitrogen	Cat#A11077
Anti-Mouse IgG, Alexa488 conjugate	Invitrogen	Cat#A11029
Anti-Rabbit IgG, RhodamineRedX conjugate	Invitrogen	Cat#R6394
Bacterial strains		
See Table S1 for a full list of bacterial strains		
Chemicals and recombinant proteins		
ATTO488-maleimide	ATTO-TEC	Cat#AD488
K27 diUb	UbiQ	Cat#UbiQ-015
K11 tetraUb	R&D Systems	Cat#UC-45–025
Deposited data		
Crystal structure of $LotA_N$	This study	PDB: 7UYG
Crystal structure of $LotA_N$ bound to K6 diUb	This study	PDB: 7UYH
Experimental models: Cell lines		
Human: HeLa-FcγRII	Laboratory of K. Arasaki	Ref[59]
Mouse: Bone marrow-derived macrophages	A/J mice	Ref[60]
Oligonucleotides		
See Table S1 for a full list of oligonucleotides		
Recombinant DNA		
See Table S1 for a full list of recombinant DNA		
Software and algorithms		
XDS	Ref[61]	Version Jan 31, 2020
CCP4i2	Ref[62]	Version 7.1.004
Aimless	Ref[63]	Version 0.7.4
SHELXC/D/E	Ref[64]	
ARP/wARP	Ref[65]	Version 8.0
Phaser	Ref[66]	Version 2.8.3
PHENIX	Ref[67]	Version 1.17.1
Coot	Ref[68]	Version 0.9
Pymol	www.pymol.org	Version 2.2.2

REAGENT or RESOURCE	SOURCE	IDENTIFIER
Prism	GraphPad	Version 9